

A Comprehensive Analysis of Text-Book-Version Afterglow Light curves of Gamma-Ray Bursts and Implication for Universal Radiation Physics of Baryonic Jets

LU-LU ZHANG,¹ SHU-QING ZHONG,² LI-PING XIN,³ AND EN-WEI LIANG^{*1}

¹Guangxi Key Laboratory for Relativistic Astrophysics, School of Physical Science and Technology, Guangxi University, Nanning 530004, People's Republic of China

²School of Science, Guangxi University of Science and Technology, Liuzhou 545006, People's Republic of China

³Key Laboratory of Space Astronomy and Technology, National Astronomical Observatories, Chinese Academy of Sciences, Beijing 100101, People's Republic of China

ABSTRACT

The standard external shock model in the thin-shell scenario predicts an onset bump in the early optical afterglow light curves of gamma-ray bursts (GRBs). We collect such a textbook-version light curve sample of 30 GRBs, and derive the jet properties from our joint fit to their X-ray and optical afterglow light curves. It is found that the distributions of the isotropic initial Lorentz factors (Γ_0), the deceleration radii (R_{dec}), and the magnetic field strength (B_0) are log-normal, but the distributions of the isotropic kinetic energy ($E_{\text{k,iso}}$), medium density (n_0), and the magnetization parameter ($\sigma_B \equiv \epsilon_B/\epsilon_e$) are tentatively bimodal. A tight $R_{\text{dec}}-B_0-\sigma_B$ relation is found. It infers a universal $\epsilon_e E_{\text{k,iso}}$ among bursts, plausibly supporting the previous argument of a universal GRB radiation energy among GRBs. A jet break is required for modeling the light curves of 26 GRBs. The distributions of the jet opening angles and the jet-corrected kinetic energies log-normally center at $\log \theta_{\text{j,c}}/\text{rad} = -1.51$ (standard deviation $\sigma = 0.27$) and $\log(E_{\text{k,j,c}}/\text{erg}) = 51.78$ ($\sigma = 0.54$), respectively. Those GRBs (19 GRBs), whose prompt gamma-ray emission is well estimated with broad energy-band observations, satisfy the previously discovered $L_{\gamma,\text{p,iso}} - E_{\text{p,z}} - \Gamma_0$ relation, and their gamma-ray radiation efficiencies log-normally distribute in the range from 0.04% to 10% with a central value of 0.42%. Such a low efficiency favors the baryonic fireball model, and the distribution of their baryon mass loading in the GRB ejecta log-normally centers at $\log(M_{\text{fb,c}}/M_\odot) = -5$ ($\sigma = 0.75$).

Keywords: gamma-ray burst; jets

1. INTRODUCTION

Gamma-ray bursts (GRBs) and their multiwavelength afterglows as amazing energetic transients are radiated from relativistic jets powered by newborn black holes or millisecond magnetars during the core collapse of rapidly spinning massive stars or the compact star mergers (Usov 1992; Woosley 1993; Fishman & Meegan 1995; Klu \acute{n} iak & Ruderman 1998; Piran 1999). The GRB survey during 1991 – 2000 by the Burst and Transient Experiment (BATSE) on board the Compton Gamma-Ray Observatory (CGRO) collected a large sample (about 2068 online triggered GRBs and 1838 offline scanned GRBs) and discovered two types of GRBs, i.e., the long-duration GRBs and short-duration GRBs (Kouveliotou et al. 1993; Fishman & Meegan 1995; Paciesas et al. 1999; Stern et al. 2001). The precise localization and discovery of multiple wavelength afterglows of GRBs since 1997 with BeppoSAX and ground-based telescopes, especially the very early afterglow observations with the X-Ray Telescope (XRT) on board the Swift mission since 2004, revolutionized our understanding of the nature of this phenomenon (Costa et al. 1997; Tavani 1997; Piran 1999; Zhang & M \acute{e} sz \acute{a} ros 2004; M \acute{e} sz \acute{a} ros 2006; Zhang et al. 2006; Gehrels et al. 2009). The GeV-TeV gamma-ray observations with the Large Area Telescope (LAT) on board the Fermi mission since 2008 and the ground-based telescopes for very high energy (VHE) since 2018, such as High Energy Stereoscopic System (H.E.S.S.), Major Atmospheric Gamma Imaging Cerenkov (MAGIC), and Large High Altitude Air Shower Observatory, further deepened our knowledge on

the radiation physics of the GRB jets (e.g., MAGIC Collaboration et al. 2019a,b; H. E. S. S. Collaboration et al. 2021; Zhang et al. 2021, 2023; Cao et al. 2023; Ren et al. 2023). More importantly, the discovery of a connection among GRBs, kilonova, and gravitational wave (GW) events since 2017, i.e., GRB 170817A/AT 2017gfo/GW170817 (e.g., Abbott et al. 2017a,b,c,d,e; Coulter et al. 2017), not only confirms that the short-duration GRBs are from the compact star mergers but also opens a new era for GRB study with multimessenger observations (e.g., Poggiani et al. 2019, 2020; Kang et al. 2023).

Although extensive investigations have been presented, the jet composition and radiation physics still remain open questions (e.g., Zhang 2011). The proposed models are classified into two groups, i.e., the matter-dominated hot fireball model and the Poynting-flux-dominated cold fireball model (e.g., Sari & Piran 1995; Zhang & Mészáros 2002, 2004; Zhang & Pe'er 2009). The matter-dominated fireball model assumes that the prompt gamma rays are emitted by the synchrotron and/or inverse Compton scattering process of the relativistic electrons that accelerated via internal shocks of the GRB fireball shells and the afterglows are emitted by the relativistic electrons accelerated via external shocks when the fireball propagates into the surrounding medium (e.g., Rees & Meszaros 1992; Meszaros & Rees 1993; Mészáros & Rees 1997; Sari et al. 1998; Sari & Piran 1999a,b; Mészáros & Rees 1999; Hu et al. 2019). The high radiation efficiency (η_γ) inferred from the observational data with the X-ray and GeV afterglows challenge the standard hot fireball model (e.g., Ioka et al. 2006; Zhang et al. 2007). The cold fireball model can provide a natural explanation for the high efficiency observed in Fermi data (e.g., Beniamini et al. 2015). In addition, the nondetection of photosphere thermal emission in broad energy-band observations for some GRBs also disfavors the hot fireball model (e.g., Zhang & Pe'er 2009; Abdo et al. 2009a; Gehrels & Razzaque 2013). Zhang & Yan (2011) proposed an internal collision-induced magnetic reconnection and turbulence (ICMART) model to explain the data of some GRBs, which can typically give a radiative efficiency of tens of percent.

The rich data of the prompt and early afterglow observations in the era of the Swift and Fermi missions since 2004 reveal a great diversity among GRBs. Thus, the issues on the jet properties and radiation physics of GRBs are still under debated. In this paper, we focus on presenting a comprehensive analysis of the GRB jet properties with a sample of “textbook” version optical light curves. These light curves apparently show a smooth afterglow onset bump, which agrees with the hot fireball model prediction in the thin-shell scenario (e.g., Rees & Meszaros 1992; Sari & Piran 1995, 1999b; Liang et al. 2010, 2013; Ghirlanda et al. 2018; Yi et al. 2020). In the framework of the standard external shock model, we present a comprehensive analysis of the jet properties of this kind of GRBs by jointly fitting the X-ray and optical afterglow light curves.

The structure of this paper is as follows. The sample selection constraints and criteria are described in Section 2. We applied the standard external forward shock (FS) model to fit the optical and X-ray afterglow data and constrained the model parameters based on the nested sampling algorithm in Section 3. The modeling results with afterglow jet properties and radiation efficiency are presented in Section 4. The correlations about the fireball deceleration and magnetization are presented in Section 5. Finally, a summary is provided in Section 6. Throughout this paper, the notations $Q_n = Q/10^n$ in cgs and $\log x = \log_{10} x$ are adopted. We take the cosmology parameters as $H_0 = 67.8 \text{ km s}^{-1} \text{ Mpc}^{-1}$, and $\Omega_M = 0.308$ (Planck et al. 2016).

2. SAMPLE SELECTION AND DATA

We select only the “textbook” version of optical light curves as predicted by the standard external shock model in the thin-shell scenario. The medium surrounding the jet is assumed to be the interstellar medium (ISM). The selection criteria are as follows.

- A clear onset bump is detected in the early optical light curve, and the decay slope post the peak time is consistent with that of the normal decay segment as predicted by the standard external model in the ISM without considering the late energy injection scenario, i.e. $0.75 < \alpha < 1.5$, where $F \propto t^{-\alpha}$ is adopted.
- X-ray afterglow observation is available.
- Redshift measurement is available.

We make an extensive search for such optical light curves from the literature. All of optical data have been corrected for Galactic extinction (Schlegel et al. 1998). The unabsorbed X-ray afterglow data are taken from the UK Swift Science Data Centre at the University of Leicester (Evans et al. 2009). We finally obtain a sample of 30 GRBs. They are listed in Table 1. Their light curves are illustrated in Figure 1.

3. MODELLING OPTICAL AND X-RAY AFTERGLOW LIGHT CURVES

3.1. GRB Afterglow Model

The dynamics of the standard GRB external FS model adopted for our analysis are outlined as (e.g., Sari et al. 1998; Huang et al. 2000; Nava et al. 2013; Zhang 2018)

$$\frac{d\Gamma}{dr} = -\frac{\Gamma(\Gamma^2 - 1)(\hat{\gamma}\Gamma - \hat{\gamma} + 1)\frac{dm}{dr}c^2 - (\hat{\gamma} - 1)\Gamma(\hat{\gamma}\Gamma^2 - \hat{\gamma} + 1)(3U/r)}{\Gamma^2[m_0 + m]c^2 + (\hat{\gamma}^2\Gamma^2 - \hat{\gamma}^2 + 3\hat{\gamma} - 2)U}, \quad (1)$$

$$\frac{dU}{dr} = (1 - \epsilon)(\Gamma - 1)c^2\frac{dm}{dr} - (\hat{\gamma} - 1)\left(\frac{3}{r} - \frac{1}{\Gamma}\frac{d\Gamma}{dr}\right)U, \quad (2)$$

where Γ is the bulk Lorentz factor of the fireball, $\hat{\gamma} = 4/3$, m_p is the proton mass, c is the speed of light, m is the swept-up mass, U is the internal energy, and ϵ is the radiation efficiency of electrons. We have $dm/dr = 4\pi r^2 n(r)m_p$, where $n(r)$ is the medium density. The continuity equation for electron distribution is (Fan et al. 2008):

$$\frac{\partial}{\partial r}\left(\frac{dN_e}{d\gamma'_e}\right) + \frac{\partial}{\partial \gamma'_e}\left[\frac{d\gamma'_e}{dr}\left(\frac{dN_e}{d\gamma'_e}\right)\right] = Q(\gamma'_e, r), \quad (3)$$

where the symbol ‘ $'$ marks the comoving frame of shock front, and

$$\frac{d\gamma'_e}{dr} = -\frac{\sigma_T}{6\pi m_e c^2} \frac{B'^2}{\beta\Gamma} [1 + Y(\gamma'_e)] \gamma'^2_e - \frac{\gamma'_e}{r} \quad (4)$$

is the cooling term of electrons, in which $B' = \sqrt{32\pi\epsilon_B n\Gamma c}$ is the internal magnetic field strength, ϵ_B denotes the fraction of the fireball internal energy allocated to the magnetic field, Y is the inverse Compton parameter, given by $Y = (-1 + \sqrt{1 + 4\epsilon_{\text{rad}}\eta_{\text{KN}}\epsilon_e/\epsilon_B})/2$ (Sari & Esin 2001; Fan et al. 2008). The cooling effects of synchrotron radiation, synchrotron self-Compton (SSC) processes, and adiabatic expansion are considered in our analysis. The shocked electrons from the medium is accelerated to a single power-law distribution in the energy space, which can be expressed as:

$$Q(\gamma'_e, r) \propto \gamma'^{-p}, \quad \gamma'_{e,\min} \leq \gamma'_e \leq \gamma'_{e,\max}. \quad (5)$$

We consider the scenario of $p > 2$ for the injected electrons, and the values of $\gamma'_{e,\min}$ and $\gamma'_{e,\max}$ are determined by

$$\gamma'_{e,\min} = \epsilon_e \frac{(p-2)}{(p-1)} \frac{m_p}{m_e} \Gamma, \quad (6)$$

$$\gamma'_{e,\max} = \sqrt{\frac{9m_e^2 c^4}{8B' q_e^3}} \quad (7)$$

where m_e and q_e are the mass and charge of the electron, respectively (e.g., Sari et al. 1998; Kumar et al. 2012).

We assume that the X-ray/optical afterglows are attributed to the synchrotron radiations of the electrons (e.g., MAGIC Collaboration et al. 2019a; Zhang et al. 2021; Fukami et al. 2022; Suda et al. 2022; Giarratana et al. 2022; Zhang et al. 2023). Assuming that the direction of the magnetic field is perpendicular to the electron velocity, the emitted spectral power of synchrotron radiation at a given frequency ν' of a single electron is given by

$$P'_e(\nu', \gamma'_e) = \frac{\sqrt{3}q_e^3 B'}{m_e c^2} F\left(\frac{\nu'}{\nu'_c}\right), \quad (8)$$

where $F(x) = x \int_x^{+\infty} K_{5/3}(k) dk$, $K_{5/3}(k)$ is the modified Bessel function of 5/3 order, and $\nu'_c = 3q_e B' \gamma'^2_e / (4\pi m_e c)$. Thus, the spectral power of synchrotron radiation of electrons $dN_e/d\gamma'_e$ at a given frequency ν' is

$$P'_{\text{syn}}(\nu') = \int_{\gamma'_{e,\min}}^{\gamma'_{e,\max}} P'_e(\nu') \frac{dN_e}{d\gamma'_e} d\gamma'_e. \quad (9)$$

In addition, the equal arrival time effect is taken into account by numerically computing the arrival times of photons (Waxman 1997),

$$t_{\text{obs}} = (1+z) \int \frac{1 - \beta \cos \Theta}{\beta c} dr \equiv \text{const}, \quad (10)$$

where Θ represents the angle between the direction of motion of a fluid element in the jet and the line of sight. We set the GRB jet as an on-axis-observed jet, i.e., $\theta_v = 0$. Assuming that the observed frequency is ν_{obs} , the frequency transformed to the comoving frame is denoted as $\nu'(\nu_{\text{obs}}) = (1+z)\nu_{\text{obs}}/\mathcal{D}$, where z is the redshift, $\mathcal{D} = 1/\Gamma(1 - \beta \cos \Theta)$ is the Doppler factor. For a detailed description of our model please refer to Zhang et al. (2023) and Ren et al. (2023).

3.2. Fitting Strategy and Results

We jointly fit the optical and X-ray light curves with the standard FS model. The early X-ray light curves are usually superimposed with bright X-ray flares from late activity of the central engine, an X-ray plateau (X-ray shallow-decayed segment) from the late energy injection of the remnant, and/or a very steep decaying segment being due to the curvature effect of the high-latitude prompt gamma rays from the emitting fireball (Zhang et al. 2006; Nousek et al. 2006). We identify a flare or a steep decay segment with a criterion of rising and/or decaying slopes being greater than 2. Inspecting the light curves shown in Figure 1, one can find that no X-ray plateau is found in these X-ray light curves but they usually start with irregular flares or a steep decaying segment, except for those that began to be observed at a late epoch ($t > 10^3$ s post the GRB trigger). Note that the XRT has several operating modes, depending on the brightness of the source being observed. Bright flares and steep decaying segments are usually observed with XRT in the windowed timing (WT) mode. Therefore, We simply exclude these WT data during our fitting. Some flares (steep decaying segments) or partial of them are observed in the photon counting (PC) mode. We also excluded these PC mode data. We marked the data that are excluded in our fit with blue color in Figure 1. The selected temporal intervals of the X-ray and optical data for our analysis are tabulated in Table 1.

The model has seven free parameters. The PyMultiNest Python package (Buchner et al. 2014) is utilized for searching the probability distributions of the model parameters in our fits, which is based on a Nested Sampling Monte Carlo algorithm for enhancing computational efficiency in a large parameter space¹. The ranges of prior parameters are listed in Table 2.

The log-likelihood functional form for evaluating the goodness of the fit is adopted as

$$\ln \mathcal{L} = -\frac{1}{2} \sum_i \left\{ \left(\frac{X_i - \hat{X}_i}{\sigma_{X,i}} \right)^2 + \ln(2\pi\sigma_{X,i}^2) + w \left[\left(\frac{O_i - \hat{O}_i}{\sigma_{O,i}} \right)^2 + \ln(2\pi\sigma_{O,i}^2) \right] \right\}, \quad (11)$$

where X_i (O_i) and $\sigma_{X,i}$ ($\sigma_{O,i}$) are the i th X-ray (optical) data point and its error, \hat{X}_i (\hat{O}_i) is the corresponding model result, and w is a weight factor. We increase the weight of the optical data by normally setting $w = 10$, because the optical data are better sampled and less contaminated by the emission from late central engine activities (flares and/or shallow decay phases/plateaus) as well as the tail emission of the prompt emission than the X-ray data.

Taking GRB 080310 as an example, Figure 2 shows the derived posterior distributions of the model parameters. The fitting curves are shown in Figure 1 and the derived model parameters are reported in Table 3. One can find that the optical and X-ray afterglow light curves can be fitted by the FS model. The derived jet properties, including the direct model parameters and the inferred quantities, are summarized in Table 4.

We discuss the derived jet properties in the next two sections. Note that the distributions of some parameters show a bimodal feature. Since the illustrated bimodal distribution feature depends on the selection of bin size, we test the bimodality with the kernel mixture modelling (KMM) algorithm in our analysis (Ashman et al. 1994). To search for possible correlations among the jet properties, we make a Pearson pair-correlation analysis and a stepwise multiple observable regression analysis. We adopt the ordinary least squares (OLS) bisector algorithm for achieving the best linear fit to derive a possible linear correlation of the data set $\{x, y\}$, $Y = \beta x + \alpha$, where β and α represent the slope and the intercept, respectively². For details on the OLS bisector algorithm please refer to Isobe et al. (1990).

4. PROPERTIES OF THE AFTERGLOW JETS

4.1. Jet Energetic, Opening Angle, and Radiation Efficiency

The distribution of the derived $E_{\text{k,iso}}$ values from our analysis is illustrated in Figure 3(a). The $\log(E_{\text{k,iso}})$ distribution displays a plausible bimodal distribution. Our fit with a model of two Gaussian functions yields the two peaks as

¹ <https://johannesbuchner.github.io/PyMultiNest/>

² The slope and intercept is given by $\beta = (\beta_1 + \beta_2)^{-1} \left[\beta_1 \beta_2 - 1 + \sqrt{(1 + \beta_1^2)(1 + \beta_2^2)} \right]$ and $\alpha = \bar{y} - \beta \bar{x}$, where i denotes the i th data point (x_i, y_i) , $\bar{x} = \frac{1}{n} \sum_{i=1}^n x_i$, $\bar{y} = \frac{1}{n} \sum_{i=1}^n y_i$, β_1 and β_2 are the OLS($X|Y$) and OLS($Y|X$), respectively. $\beta_1 = S_{xy}/S_{xx}$, $\beta_2 = S_{yy}/S_{xy}$, where $S_{xx} = \sum_{i=1}^n (x_i - \bar{x})^2$, $S_{yy} = \sum_{i=1}^n (y_i - \bar{y})^2$, and $S_{xy} = \sum_{i=1}^n (x_i - \bar{x})(y_i - \bar{y})$.

$\log(E_{k,\text{iso},c_1}/\text{erg}) = 53.81$ and $\log(E_{k,\text{iso},c_2}/\text{erg}) = 55.34$. Most of the bursts (22/30) are of the high- $E_{k,\text{iso}}$ group. We compare the distribution of $\log(E_{k,\text{iso}})$ with a sample of GRBs whose optical and X-ray afterglows can be explained with the FS model in the ISM scenario reported by Wang et al. (2015). As shown in Figure 3(a), the $\log(E_{k,\text{iso}})$ distributions of the two samples cover almost the same range, but no clear bimodal distribution is found in the sample from Wang et al. (2015). Since the apparent bimodal distribution depends on the selection of the bin size, we check the bimodality of the $\log(E_{k,\text{iso}})$ distribution derived from our analysis with the KMM test, which yields a p -value of 0.005. Hence the bimodality is only marginally claimed.

The jet opening angles are obtained from our fits for 26 GRBs among the 30 bursts³. The distribution of the derived θ_j values is shown in Figure 3(c). It peaks at $\log(\theta_j/\text{rad}) = -1.4$ ($\theta_j = 2.3^\circ$) and the central value $\log(\theta_{j,c}/\text{rad}) = -1.51$ ($\theta_{j,c} = 1.8^\circ$). The peak value is almost consistent with that reported by Wang et al. (2015). We calculate the jet-corrected kinetic energy as $E_{k,j} = E_{k,\text{iso}}(1 - \cos\theta_j)$, and show its distribution in Figure 3(d). It is found that $E_{k,j} \in \{10^{50} \sim 10^{53}\}$ erg and the $\log(E_{k,j})$ distribution can be fit with a Gaussian function, which yields a central value of $\log(E_{k,j,c}/\text{erg}) = 51.78$ and a standard deviation (σ) as 0.54. The R^2 of the fit is 0.98.

Broadband observations with Fermi Gamma-ray Burst Monitor (GBM, 8 keV-40 MeV), Konus-Wind (~ 20 keV – 20 MeV for the triggered mode and ~ 20 keV – 1.5 MeV for the waiting mode; Tsvetkova et al. 2021), or Suzaku Wide-band All-sky Monitor (WAM, 50 keV – 5 MeV, Krimm et al. 2009) telescopes are available for 19 out of the 30 bursts⁴. Their isotropic prompt gamma-ray energy ($E_{\gamma,\text{iso}}$) can be robustly estimated with the observations of these telescopes. We calculate their $E_{\gamma,\text{iso}}$ in the $1 - 10^4$ keV band and show $\log E_{\gamma,\text{iso}}$ as a function of $\log E_{k,\text{iso}}$ in Figure 3(f). It is found that $E_{\gamma,\text{iso}}$ is not correlated with $E_{k,\text{iso}}$ and the $\log E_{\gamma,\text{iso}}$ distribution does not show a bimodal feature as that seen in the $\log E_{k,\text{iso}}$ distribution. The $\log E_{\gamma,\text{iso}}$ distribution is clustered around $\log(E_{\gamma,\text{iso}}/\text{erg}) \sim 53$. Our fit with a Gaussian function yields $\log(E_{\gamma,\text{iso},c}/\text{erg}) = 52.96$ ($\sigma = 0.37$). Deriving the jet gamma-ray energy ($E_{\gamma,j}$) by making geometrical correction with the derived jet opening angle, it is found that $E_{\gamma,j} \in \{10^{48}, 7.2 \times 10^{50}\}$ erg. The $\log E_{\gamma,j}$ distribution can be fitted with a Gaussian function, yielding $\log E_{\gamma,j,c}/\text{erg} = 49.47$ ($\sigma=0.87$). The R^2 of the fit is 0.99. The normal distributions of $\log(E_{\gamma,j})$ and $\log(E_{k,j})$ are shown in Figure 3(d). We should note that the distributions are similar to those reported by Frail et al. (2001) and Berger et al. (2003), who proposed a standard energy reservoir among GRB jets.

The radiation efficiency gives insights into the radiation physics and composition of the GRB fireball (e.g., Piran 1999). The hot fireball model predicts that the radiation efficiency is lower than 10% (e.g., Kumar 1999; Panaiteescu et al. 1999; Fan & Piran 2006). The inferred high η_γ ($> 10\%$ even up to 90%; e.g., Zhang et al. 2007; Wang et al. 2015) using the X-ray and GeV gamma-ray afterglow data is a great challenge to the standard external shock model (e.g., Ioka et al. 2006; Zhang et al. 2007). We calculate the GRB radiative efficiency by $\eta_\gamma = E_{\gamma,\text{iso}}/(E_{\gamma,\text{iso}} + E_{k,\text{iso}})$. Figure 3(e) shows the distribution of $\log(\eta_\gamma/\%)$, which can be fitted with a Gaussian function. One can find that the $\log(\eta_\gamma/\%)$ values range from -1.4 to 1 ($\eta_\gamma = 0.04\% - 6.73\%$). The median and mode of the $\log(\eta_\gamma/\%)$ distribution are -0.27 and -0.35 (corresponding to $\eta_\gamma = 0.54\%$ and 0.42%). The radiative efficiencies of GRBs 051109, 051111, 120729A and 140629A are lower than or equal to 0.1%. We also mark the lines for $\eta_\gamma = 0.04\%$, 1% , and 10% in Figure 3(f). The derived low radiative efficiency for the bursts in our sample favors the viewpoint that the jets of these GRBs are matter-dominated.

4.2. The Fireball Initial Lorentz Factor, Medium Density, and Deceleration Radius

In the initial stage, the fireball evolves through a radiation-dominated acceleration phase to a matter-dominated “coasting” phase. During the coasting phase, the initial Lorentz factor (Γ_0) remains approximately constant until the fireball accumulates a significant amount of mass from the surrounding medium and begins to decelerate. The observed afterglow onset peak marks the deceleration of the GRB fireball in the thin-shell scenario of the standard fireball model (e.g., Sari & Piran 1999b; Liang et al. 2010, 2013). Hence, Γ_0 is sensitive to the peak time of the afterglow light curves. The derived Γ_0 values of most bursts (26/30) are greater than 100, being consistent with the expectation of the GRB fireball model for avoiding the compactness problem (e.g., Lithwick & Sari 2001; Abdo et al. 2009a; Zhang et al. 2022). The $\log(\Gamma_0)$ distribution derived from our fits is shown in Figure 4(a). Although the $\log(\Gamma_0)$ distribution can be roughly fitted with a Gaussian function, i.e., $\log \Gamma_{0,c} = 2.63$ ($\sigma = 0.27$), it shows a sharp cut at the right side. This would be due to our sample selection effect. The GRBs included in our analysis are selected with

³ The fit to the lightcurves of GRBs 070411, 120815A, 141221A and 181110A are not required to assign a jet opening angle.

⁴ GRBs that only detected by *Swift*/BAT instrument are excluded. They are GRBs 060526, 070411, 071010A, 071031, 071112C, 080310, 080603, 080710, 090313, 120815A, and 170519A.

the detection of the optical afterglow onset peak. The deceleration time of extremely bright GRBs occurs very early, which can often be missed by observation or affected by the prompt optical emission and the optical emission of the reverse shock (e.g., Racusin et al. 2008; Xin et al. 2023). In fact, the Lorentz factors of some GRBs estimated with the Fermi/LAT observations are greater than 1000, which is essential to prevent high-energy photons from undergoing annihilation through the creation of e^\pm pairs (e.g., Abdo et al. 2009a,b,c; Ioka 2010).

Ghirlanda et al. (2018) calculated the Γ_0 values of the bursts with the detection of the optical onset bump in both the ISM and wind medium scenarios. In the ISM scenario, they adopted $n_0 = 1 \text{ cm}^{-3}$ and estimated the $E_{\text{k,iso}}$ value with $E_{\text{k,iso}} = E_{\gamma,\text{iso}}/\eta_\gamma$, where η_γ is assumed to be a universal value of 20% for all bursts. We compare the $\log(\Gamma_0)$ distributions between ours and that calculated with the data reported by Ghirlanda et al. (2018) in Figure 4(a). It is found that the central value Γ_0 derived from our analysis is larger than that from Ghirlanda et al. (2018) by a factor of ~ 2 , i.e., $\Gamma_0 = 426^{+794}_{-229}$ (1σ range in log-scale) vs. $\Gamma_0 = 204^{+389}_{-107}$. The discrepancy is mostly due to the difference of n_0 and η_γ values since $\Gamma_0 \propto E_{\text{k,iso}}^{1/8} n_0^{1/8} t_{\text{peak},z}^{-3/8}$. As shown in Figure 3, the η_γ values derived from our analysis are mostly in the range of $0.04\% \sim 10\%$ with a typical value of $\sim 0.4\%$. It is smaller than that adopted by Ghirlanda et al. (2018) by a factor of 50. This leads to an underestimation of the Γ_0 value by a factor of $50^{1/8} \sim 1.6$. This can reasonably explain the discrepancy between our results and those reported by Ghirlanda et al. (2018).

Furthermore, we calculate the baryon mass loading in the GRB ejecta by $M_{\text{fb}} = E_{\text{k,j}}/(\Gamma_0 c^2)$. Figure 4(b) shows the $\log(M_{\text{fb}}/M_\odot)$ distribution, which covers from $6.54 \times 10^{-7} M_\odot$ to $2.02 \times 10^{-5} M_\odot$ with a mode of $M_{\text{fb,p}} = 1.48 \times 10^{-5} M_\odot$. Ghirlanda et al. (2018) derived the $\log(M_{\text{fb}}/M_\odot)$ distribution for a sample of GRBs with the detection of the optical afterglow onset bump. The $\log(M_{\text{fb}}/M_\odot)$ distribution derived from their analysis mainly covers the range of $10^{-7} \sim 10^{-4} M_\odot$, being averagely smaller than that derived from our analysis by a factor of 4, as shown in Figure 4(b). We should note that Ghirlanda et al. (2018) estimated the $E_{\text{k,j}}$ values with $E_{\text{k,j}} = E_{\gamma,\text{iso}}(1 - \cos\theta_j)/\eta_\gamma$ by taking $\theta_j = 5^\circ$ and $\eta_\gamma = 20\%$ for all bursts. The $E_{\text{k,j}}$ and η_γ values in our analysis are derived from theoretical modeling. This would result in the difference between ours and that reported by Ghirlanda et al. (2018).

The derived medium density among the bursts ranges from 10^{-3} to 10^3 cm^{-3} , as shown in Figure 4(c). Its distribution shows a clear bimodal feature, with a separation at $\log(n_0/\text{cm}^{-3}) \sim -0.1$. The low-density group (12/30 of bursts) narrowly cluster at $\log(n_0/\text{cm}^{-3}) = -2.5$, and the high-density group (18/30 of bursts) normally peaks at around $\log(n_0/\text{cm}^{-3}) = 1$. Our fit with a bimodal model yields $\log(n_{0,c1}/\text{cm}^{-3}) = -2.5$ ($\sigma = 0.5$) and $\log(n_{0,c2}/\text{cm}^{-3}) = 1.0$ ($\sigma = 1.3$). The bimodality test with the KMM algorithm gives a p -value of 0.037. The bimodality $\log n_0$ distribution suggests that two groups of GRBs should be in difference environments (e.g., Fruchter et al. 2006). The GRBs of the high-density (or low-density) group may be close to (or far away from) the star formation regions of their host galaxies.

The fireball is decelerated by the surrounding medium. The deceleration radius is defined as

$$R_{\text{dec}} = \left(\frac{3E_{\text{k,iso}}}{2\pi\hat{\gamma}\Gamma_0^2 n_0 m_p c^2} \right)^{1/3} \approx (6.2 \times 10^{16} \text{ cm}) E_{\text{k,iso},52}^{1/3} \Gamma_{0,2}^{-2/3} n_0^{-1/3}. \quad (12)$$

The derived R_{dec} distribution is shown in Figure 4(d). It is found that the R_{dec} distribution covers the range of $2.22 \times 10^{16} - 3.57 \times 10^{18} \text{ cm}$ and it is well fitted with a log-normal function, i.e., $\log(R_{\text{dec},17,c}/\text{cm}) = 0.59$ ($\sigma = 0.56$).

It is interesting that the derived R_{dec} distribution is log-normal, although the n_0 distributions are tentatively bimodal. We suspect that this results from the degeneration of $E_{\text{k,iso}}$ and n_0 in our light curve fitting. We first check whether $E_{\text{k,iso}}$ and n_0 have degenerated in the MCMC fit for individual GRBs, but do not find clear degeneration feature that shows as a narrow band in the probability contour in the $\log E_{\text{k,iso}} - \log n_0$ plane. Second, we examine the correlations of the two parameters among the bursts, but we do not find any correlation, as shown in Figure 5(a). Therefore, the bimodal distribution of n_0 should be not due to the degeneration of $E_{\text{k,iso}}$ and n_0 . Third, the log-normal distribution of R_{dec} suggests a correlation among $E_{\text{k,iso}}$, n_0 , and Γ_0 based on Eq. 12. We further test the correlation between the ratio of $\varepsilon \equiv E_{\text{k,iso}}/n_0$ and $\Gamma_{0,2}^2$, where ε is in sense of the isotropic kinetic energy per particle density. Figure 5(b) shows ε as a function of $\Gamma_{0,2}^2$. It is found that the two quantities are tightly correlated. The multiple linear regression analysis gives a correlation coefficient of 0.88 and a chance probability of $p < 10^{-4}$. The best fit with the OLS bisector algorithm yields a relation of $\varepsilon = (3.08 \pm 0.24) \log(\Gamma_{0,2}^2) \pm (0.31 \pm 0.31)$. The dispersion of the relation is $\delta = 1.19$. This correlation infers a quasi-universal R_{dec} (a log-normal distribution of R_{dec}) since $R_{\text{dec}} \propto \varepsilon^{1/3} \Gamma_{0,2}^{-2/3}$.

4.3. The jet energy equipartition and composition

The internal energy of the fireball is assumed to be carried by the electrons, protons, and magnetic field with the electron equipartition parameter ϵ_e and the magnetic equipartition parameter ϵ_B (e.g., Zhang 2011). The distribution

of $\log(\epsilon_e)$ for the bursts in our sample is shown in Figure 6(a). One can observe that the $\log(\epsilon_e)$ distribution illustrates two peaks at -2.39 ($\sigma = 0.36$) and -0.95 ($\sigma = 0.39$), which are derived from our bimodal function fit ($R^2 = 0.88$). The p -value of the KMM test is 0.014, and the inferred two peaks are at -2.40 and -0.94 . The broad $\log(\epsilon_e)$ distribution might suggest the efficiency of the electron acceleration among bursts is dramatically different. The low- ϵ_e group likely suggests the existence of a scenario in which the electrons are unable to be efficiently accelerated by the GRB blast wave or completely radiative even when electrons are in the fast-cooling regime (e.g., Gao et al. 2013). This may lead to a low-value η_γ (e.g., Wang et al. 2015). We examine the correlation between ϵ_e and η_γ , as shown in Figure 7. Our analysis with the OLS bisector algorithm gives a relation of $\log(\eta_\gamma) = (0.93 \pm 0.15) \log(\epsilon_e) + (1.66 \pm 0.35)$, and the Pearson correlation coefficient is $r = 0.64$. The dispersion of this relation is $\delta = 0.50$. This relation suggests that fireballs with a lower ϵ_e value tend to have a smaller gamma-ray radiation efficiency η_γ .

The $\log(\epsilon_B)$ distribution spans a wide range from -7 to -1.5 with a mode of -3.32 and a median of $\log(\epsilon_{B,c}) = -4.09 \pm 0.14$, as shown in Figure 6(b). This statistically agrees with that reported by the literature (Santana et al. 2014; Japelj et al. 2014; Santana et al. 2014; Gao et al. 2015; Wang et al. 2015). Adopting a ratio $\sigma_B = \epsilon_B/\epsilon_e$ as a measurement of the fireball magnetization, we find that the $\log \sigma_B$ values range in $[-5.5, 0.5]$ and its distribution illustrates as a plausible bimodal distribution that peaks at $\log \sigma_{B,c_1} = -4.3 \pm 0.3$ and $\log \sigma_{B,c_2} = -1.3 \pm 0.1$, as shown in Figure 6(c). The p -value of the KMM test is 0.09. We also calculate the initial magnetic field strength of the fireball with

$$B_0 = (32\pi m_p \epsilon_B n_0)^{1/2} \Gamma_0 c. \quad (13)$$

The distribution of $\log(B_0/\text{Gs})$ is present in Figure 6(e). It spans from -1.6 to 1.2 and can be fitted with a Gaussian function, i.e., $\log(B_{0,c}/\text{Gs}) = -0.17$ and $\sigma = 0.54$.

The electrons are assumed to be accelerated by the shocks in the jets. The derived power-law indices p of the electron spectrum cover the range of from 2.05 to 2.6, but a large fraction of them narrowly cluster at [2.05, 2.1], as shown in Figure 6(d). The derived electron spectra of these bursts are systematically harder than that predicted by the particle acceleration via shocks (e.g., Achterberg et al. 2001; Lemoine & Pelletier 2003).

5. CORRELATION ANALYSIS OF THE JET PROPERTIES

5.1. $R_{\text{dec}} - \sigma_B - B_0$ Relation

The deceleration of the fireball is a dynamic feature. We first explore whether the deceleration radius R_{dec} is correlated with the magnetization of the jet. Interestingly, we find a tentative correlation between R_{dec} and σ_B , as shown in Figure 8(a). Our fit gives

$$\log(R_{\text{dec},17}) = (0.38 \pm 0.05) \log(\sigma_B) + (1.41 \pm 0.11), \quad (14)$$

with a Pearson correlation coefficient of $r = 0.65$ and a chance probability p -value $< 10^{-4}$, the dispersion of the relation is $\delta = 0.47$. This relation suggests that a fireball with a higher degree of magnetization tends to have a larger deceleration radius, hence a longer deceleration timescale. We also search the relation of $R_{\text{dec},17}$ to the initial magnetic field strength B_0 . We find that B_0 is anticorrelated with $R_{\text{dec},17}$ in Figure 8(b), e.g.,

$$\log(B_0/\text{Gs}) = (-0.89 \pm 0.12) \log(R_{\text{dec},17}) + (0.31 \pm 0.09). \quad (15)$$

Furthermore, we make stepwise multiple variable regression analysis among $R_{\text{dec},17}$, B_0 , and σ_B . We obtain a $R_{\text{dec},17}^r(B_0, \sigma_B)$ relation as

$$\log(R_{\text{dec},17}^r) = (1.00 \pm 0.05) - (0.83 \pm 0.06) \log(B_0) + (0.26 \pm 0.02) \log(\sigma_B). \quad (16)$$

The regression analysis yields an F-test probability is 204.25. Figure 8(c) shows $R_{\text{dec},17}^r$ as a function of $R_{\text{dec},17}$. The Pearson linear correlation coefficient of the two quantities is $r = 0.97$ and the chance probability is $p = 0$. Our best linear fit gives $R_{\text{dec},17}^r = (0.97 \pm 0.04)R_{\text{dec},17} \pm (0.02 \pm 0.04)$, and the standard deviation is $\delta = 0.16$. These results indicate that the $R_{\text{dec},17}^r(B_0, \sigma_B)$ relation is very tight. Note that, GRBs 060526 and 080603A, which are masked with red stars in Figure 8(a), are far away from the 95% confidence band of the $\log R_{\text{dec}} - \log \sigma_B$ relation. GRB 060526 has the smallest R_{dec} and GRB 080603A has the smallest σ_B value among the bursts in our sample. They do not display other unique characteristics of their prompt and afterglow emission. It is interesting that they are still within the 95% confidence band of the $R_{\text{dec},17}^r(B_0, \sigma_B)$ relation.

Apparently, the tight $R_{\text{dec},17}^r(B_0, \sigma_B)$ relation indicates that the deceleration radius depends on the magnetization of the fireball. The physics behind this relation is of our interest. Note that $R_{\text{dec},17}^r$, B_0 , and σ_B are not observational data, but are calculated with the model parameters derived from our fits. Based on Eqs. (12) and (13), we have $R_{\text{dec}} \propto (B_0^{-2}\sigma_B)^{1/3}(\epsilon_e E_{\text{k,iso}})^{1/3}$, i.e., $\log R_{\text{dec}} \propto -\frac{2}{3}\log B_0 + \frac{1}{3}\log\sigma_B + \frac{1}{3}\log(\epsilon_e E_{\text{k,iso}})$. This is roughly consistent with Eq. 16 if $\epsilon_e E_{\text{k,iso}}$ is a constant among bursts. Thus, this relation hints that a certain fraction of the kinetic energy carried by the electrons ($\epsilon_e E_{\text{k,iso}}$) is almost constant.

5.2. $L_{\gamma,p,\text{iso}} - E_{p,z} - \Gamma_0$ Relation

Liang et al. (2015) discovered a tight $L_{\gamma,\text{iso},52}^r(E_{p,z}, \Gamma_0)$ relation, where $E_{p,z} = E_p(1+z)$. This relation is incorporated in both the $L_{\gamma,p,\text{iso}} - E_{p,z}$ (Amati et al. 2002; Liang et al. 2004) and $L_{\gamma,p,\text{iso}} - \Gamma_0$ relations (Liang et al. 2010), and significantly reduces the intrinsic scatters of the $L_{\gamma,\text{iso}} - E_{p,z}$ and $L_{\gamma,\text{iso}} - \Gamma_0$ relations. Extremely bright GRBs (e.g., GRB 221009A, Lan et al. 2023) and other bright GRBs with detection of TeV/sub-TeV gamma-ray afterglows (GRBs 180720B, 190114C, 190829A, 201015A, 201216C; Huang et al. 2020; Zhang et al. 2023) well satisfy this relation. Note that Liang et al. (2015) calculated the Γ_0 value with $\Gamma_0 \propto (n_0\eta_\gamma)^{-1/8}(E_{\gamma,\text{iso},52}t_{p,z}^{-3})^{1/8}$ by adopting universal values of n_0 and η_γ among bursts, i.e., $n_0 = 1 \text{ cm}^{-3}$ and $\eta_\gamma = 0.2$. As shown in this analysis, these values are diverse among bursts. We examine whether the GRBs in our sample agree with this relation by using the Γ_0 values derived from our analysis. We use only those GRBs whose their $L_{\gamma,p,\text{iso}}$ and $E_{p,z}$ values can be robustly derived from observations with broadband gamma-ray instruments as mentioned above⁵. The $L_{\gamma,\text{iso},52}^r(E_{p,z}, \Gamma_0)$ relation reported by Liang et al. (2015) is written as⁶

$$L_{\gamma,\text{iso},52}^r(E_{p,z}, \Gamma_0) = 10^{-6.38 \pm 0.35} (E_{p,z}/\text{keV})^{1.34 \pm 0.14} \Gamma_0^{1.32 \pm 0.19} \quad (17)$$

and its dispersion is illustrated in Figure 9 by the correlation of $L_{\gamma,p,\text{iso},52}^r - L_{\gamma,\text{iso},52}$. We calculate the $L_{\gamma,p,\text{iso},52}^r$ values with Eq. 17 by using the Γ_0 values derived from our analysis. Our results are compared with those reported by Liang et al. (2015) in the $L_{\gamma,p,\text{iso},52}^r - L_{\gamma,\text{iso},52}$ plane. One can observe that the $L_{\gamma,\text{iso},52}^r(E_{p,z}, \Gamma_0)$ relation is confirmed by our results, although the data points have large uncertainties that are attributed to the large uncertainties of Γ_0 from our fits to the light curves.

6. SUMMARY

By jointly fitting the optical and X-ray afterglow light curves of a sample of 30 GRBs that have detected of an early onset bump in their optical afterglow with a standard external shock model, we derive the jet properties of these bursts. They are summarized below.

- The distribution of $\log(\theta_j)$ for 26 out of the 30 bursts normally peaks at $\log(\theta_{j,c}/\text{rad}) = -1.4$ (i.e., $\theta_{j,c} = 2.3^\circ$), and the distributions of $\log E_{\text{k,j}}$ and $\log E_{\gamma,j}$ (for 19 out of the 26 bursts) normally peaks at $\log(E_{\text{k,j,c}}/\text{erg}) = 51.78$ and $\log(E_{\gamma,j,c}/\text{erg}) = 49.47$. These results are consistent with the idea of a standard energy reservoir among GRBs previously reported by Frail et al. (2001) and Berger et al. (2003), although the derived $E_{\gamma,j,c}$ of our sample is lower than that reported in Frail et al. (2001) by about 1 order of magnitude.
- The inferred radiation efficiencies of the 30 bursts are lower than 10% and even down to 0.04%, being consistent with the model prediction for the material-dominated jet scenario. The initial magnetic field strength B_0 has a normal distribution after taking the logarithm, yielding the central value is $B_{0,c} = 0.68 \text{ Gs}$. The normal distribution of $\log(M_{\text{fb}}/M_\odot)$ peaks concentrated at $M_{\text{fb},p} = 1.48 \times 10^{-5} M_\odot$. Measuring the fireball magnetization with $\sigma_B = \epsilon_B/\epsilon_e$, we find $\sigma_B < 1$ for 90% of the GRBs in our sample, suggesting a relatively weak magnetization of these GRBs. Interestingly, we find a tight correlation of $R_{\text{dec},17}^r = 10^{0.10 \pm 0.05} B_0^{-0.83 \pm 0.06} \sigma_B^{0.26 \pm 0.02}$. This relation infers a universal kinetic energy carried by the electrons ($\epsilon_e E_{\text{k,iso}}$) among the GRBs.
- The distributions of the initial Lorentz factor and deceleration radius of the fireball are normally peak at $\log(\Gamma_{0,c}) = 2.63$ and $\log(R_{\text{dec},c})/\text{cm} = 17.59$, although the circumburst density shows a bimodal distribution with separation at 0.1 cm^{-3} . Adopting the Γ_0 values derived from analysis, we confirm the tight $L_{\text{p,iso}} - E_{p,z} - \Gamma_0$ relation previously reported by Liang et al. (2015).

⁵ We excluded the following GRBs from the sample due to the lack of the value of E_p or $L_{\text{p,iso}}$: GRBs 071112C, 090313, 120729A, 120815A, 160203A and 170519A. At the same time, we calculated the isotropic peak luminosity $L_{\text{p,iso}}$ using the data from Fermi/GBM, analysis data via GBM Data Tools (Goldstein et al. 2021), which included GRBs 080810, 081008, 081109A, 130610A and 141221A.

⁶ Adopting the multiply regression analysis, we also derive this relation from the data reported in this sample as $L_{\gamma,p,\text{iso},52}^r = 10^{-5.26 \pm 1.11} (E_{p,z}/\text{keV})^{0.94 \pm 0.35} \Gamma_0^{1.16 \pm 0.41}$. The derived parameters are slightly different from those reported by Liang et al. (2015).

ACKNOWLEDGMENTS

We are deeply grateful for the insightful comments provided by the referee. This work used data and software provided by the Fermi Science Support Center and data supplied by the UK Swift Science Data Centre at the University of Leicester. This work is supported by the National Natural Science Foundation of China (Grant No.12133003). S.Q.Z. acknowledges support from the National Natural Science Foundation of China (grant No. 12247144), China Postdoctoral Science Foundation (grant Nos. 2021TQ0325 and 2022M723060) and the starting Foundation of Guangxi University of Science and Technology (grant No. 24Z17).

Software: Matplotlib (Hunter 2007), PyMultiNest (Buchner 2016), Numpy (Harris et al. 2020), GBM Data Tools (Goldstein et al. 2021), Astropy (Astropy Collaboration et al. 2013)

REFERENCES

- Abbott, B. P., Abbott, R., Abbott, T. D., et al. 2017a, ApJL, 850, L39, doi: [10.3847/2041-8213/aa9478](https://doi.org/10.3847/2041-8213/aa9478)
- . 2017b, ApJL, 850, L40, doi: [10.3847/2041-8213/aa93fc](https://doi.org/10.3847/2041-8213/aa93fc)
- . 2017c, ApJL, 848, L13, doi: [10.3847/2041-8213/aa920c](https://doi.org/10.3847/2041-8213/aa920c)
- . 2017d, ApJ, 841, 89, doi: [10.3847/1538-4357/aa6c47](https://doi.org/10.3847/1538-4357/aa6c47)
- . 2017e, PhRvD, 96, 022001, doi: [10.1103/PhysRevD.96.022001](https://doi.org/10.1103/PhysRevD.96.022001)
- Abdo, A. A., Ackermann, M., Arimoto, M., et al. 2009a, Science, 323, 1688, doi: [10.1126/science.1169101](https://doi.org/10.1126/science.1169101)
- Abdo, A. A., Ackermann, M., Ajello, M., et al. 2009b, Nature, 462, 331, doi: [10.1038/nature08574](https://doi.org/10.1038/nature08574)
- . 2009c, ApJL, 706, L138, doi: [10.1088/0004-637X/706/1/L138](https://doi.org/10.1088/0004-637X/706/1/L138)
- Achterberg, A., Gallant, Y. A., Kirk, J. G., & Guthmann, A. W. 2001, MNRAS, 328, 393, doi: [10.1046/j.1365-8711.2001.04851.x](https://doi.org/10.1046/j.1365-8711.2001.04851.x)
- Amati, L., Frontera, F., Tavani, M., et al. 2002, A&A, 390, 81, doi: [10.1051/0004-6361:20020722](https://doi.org/10.1051/0004-6361:20020722)
- Ashman, K. M., Bird, C. M., & Zepf, S. E. 1994, AJ, 108, 2348, doi: [10.1086/117248](https://doi.org/10.1086/117248)
- Astropy Collaboration, Robitaille, T. P., Tollerud, E. J., et al. 2013, A&A, 558, A33, doi: [10.1051/0004-6361/201322068](https://doi.org/10.1051/0004-6361/201322068)
- Atteia, J. L., Heussaff, V., Dezelay, J. P., et al. 2017, ApJ, 837, 119, doi: [10.3847/1538-4357/aa5ffa](https://doi.org/10.3847/1538-4357/aa5ffa)
- Beniamini, P., Nava, L., Duran, R. B., & Piran, T. 2015, MNRAS, 454, 1073, doi: [10.1093/mnras/stv2033](https://doi.org/10.1093/mnras/stv2033)
- Berger, E., Kulkarni, S. R., & Frail, D. A. 2003, ApJ, 590, 379, doi: [10.1086/374892](https://doi.org/10.1086/374892)
- Beskin, G. M., Oganesyan, G., Greco, G., & Karpov, S. 2015, Astrophysical Bulletin, 70, 400, doi: [10.1134/S1990341315040033](https://doi.org/10.1134/S1990341315040033)
- Buchner, J. 2016, PyMultiNest: Python interface for MultiNest, Astrophysics Source Code Library, record ascl:1606.005. <http://ascl.net/1606.005>
- Buchner, J., Georgakakis, A., Nandra, K., et al. 2014, A&A, 564, A125, doi: [10.1051/0004-6361/201322971](https://doi.org/10.1051/0004-6361/201322971)
- Butler, N. R., Li, W., Perley, D., et al. 2006, ApJ, 652, 1390, doi: [10.1086/508624](https://doi.org/10.1086/508624)
- Cano, Z., Bersier, D., Guidorzi, C., et al. 2011, MNRAS, 413, 669, doi: [10.1111/j.1365-2966.2010.18164.x](https://doi.org/10.1111/j.1365-2966.2010.18164.x)
- Cano, Z., de Ugarte Postigo, A., Pozanenko, A., et al. 2014, A&A, 568, A19, doi: [10.1051/0004-6361/201423920](https://doi.org/10.1051/0004-6361/201423920)
- Cao, Z., Aharonian, F., An, Q., et al. 2023, Science Advances, 9, eadj2778, doi: [10.1126/sciadv.adj2778](https://doi.org/10.1126/sciadv.adj2778)
- Cenko, S. B., Kasliwal, M., Harrison, F. A., et al. 2006, ApJ, 652, 490, doi: [10.1086/508149](https://doi.org/10.1086/508149)
- Costa, E., Frontera, F., Heise, J., et al. 1997, Nature, 387, 783, doi: [10.1038/42885](https://doi.org/10.1038/42885)
- Coulter, D. A., Foley, R. J., Kilpatrick, C. D., et al. 2017, Science, 358, 1556, doi: [10.1126/science.aap9811](https://doi.org/10.1126/science.aap9811)
- Covino, S., D’Avanzo, P., Klotz, A., et al. 2008, MNRAS, 388, 347, doi: [10.1111/j.1365-2966.2008.13393.x](https://doi.org/10.1111/j.1365-2966.2008.13393.x)
- Crisp, H., Gendre, B., Howell, E. J., & Coward, D. 2021, MNRAS, 504, 716, doi: [10.1093/mnras/stab916](https://doi.org/10.1093/mnras/stab916)
- Evans, P. A., Beardmore, A. P., Page, K. L., et al. 2009, MNRAS, 397, 1177, doi: [10.1111/j.1365-2966.2009.14913.x](https://doi.org/10.1111/j.1365-2966.2009.14913.x)
- Fan, Y., & Piran, T. 2006, MNRAS, 369, 197, doi: [10.1111/j.1365-2966.2006.10280.x](https://doi.org/10.1111/j.1365-2966.2006.10280.x)
- Fan, Y.-Z., Piran, T., Narayan, R., & Wei, D.-M. 2008, MNRAS, 384, 1483, doi: [10.1111/j.1365-2966.2007.12765.x](https://doi.org/10.1111/j.1365-2966.2007.12765.x)
- Ferrero, P., Kann, D. A., Klose, S., et al. 2008, in American Institute of Physics Conference Series, Vol. 1000, Gamma-ray Bursts 2007, ed. M. Galassi, D. Palmer, & E. Fenimore, 257–260, doi: [10.1063/1.2943458](https://doi.org/10.1063/1.2943458)
- Fishman, G. J., & Meegan, C. A. 1995, ARA&A, 33, 415, doi: [10.1146/annurev.aa.33.090195.002215](https://doi.org/10.1146/annurev.aa.33.090195.002215)
- Fitzpatrick, G., & Pelassa, V. 2013, GRB Coordinates Network, 14858, 1
- Frail, D. A., Kulkarni, S. R., Sari, R., et al. 2001, ApJL, 562, L55, doi: [10.1086/338119](https://doi.org/10.1086/338119)

- Fruchter, A. S., Levan, A. J., Strolger, L., et al. 2006, *Nature*, 441, 463, doi: [10.1038/nature04787](https://doi.org/10.1038/nature04787)
- Fukami, S., Berti, A., Loporchio, S., et al. 2022, in 37th International Cosmic Ray Conference, 788, doi: [10.22323/1.395.0788](https://doi.org/10.22323/1.395.0788)
- Gao, H., Lei, W.-H., Zou, Y.-C., Wu, X.-F., & Zhang, B. 2013, *NewAR*, 57, 141, doi: [10.1016/j.newar.2013.10.001](https://doi.org/10.1016/j.newar.2013.10.001)
- Gao, H., Wang, X.-G., Mészáros, P., & Zhang, B. 2015, *ApJ*, 810, 160, doi: [10.1088/0004-637X/810/2/160](https://doi.org/10.1088/0004-637X/810/2/160)
- Gehrels, N., Ramirez-Ruiz, E., & Fox, D. B. 2009, *ARA&A*, 47, 567, doi: [10.1146/annurev.astro.46.060407.145147](https://doi.org/10.1146/annurev.astro.46.060407.145147)
- Gehrels, N., & Razzaque, S. 2013, *Frontiers of Physics*, 8, 661, doi: [10.1007/s11467-013-0282-3](https://doi.org/10.1007/s11467-013-0282-3)
- Gendre, B., Orange, N. B., Moore, E., et al. 2022, *ApJ*, 929, 16, doi: [10.3847/1538-4357/ac561e](https://doi.org/10.3847/1538-4357/ac561e)
- Ghirlanda, G., Nappo, F., Ghisellini, G., et al. 2018, *A&A*, 609, A112, doi: [10.1051/0004-6361/201731598](https://doi.org/10.1051/0004-6361/201731598)
- Giarratana, S., Rhodes, L., Marcote, B., et al. 2022, *A&A*, 664, A36, doi: [10.1051/0004-6361/202142919](https://doi.org/10.1051/0004-6361/202142919)
- Goldstein, A., Cleveland, W. H., & Kocevski, D. 2021, Fermi GBM Data Tools: v1.1.0. <https://fermi.gsfc.nasa.gov/ssc/data/analysis/gbm>
- Golenetskii, S., Aptekar, R., Mazets, E., et al. 2005a, GRB Coordinates Network, 4030, 1
- . 2005b, GRB Coordinates Network, 4238, 1
- . 2006, GRB Coordinates Network, 4989, 1
- . 2008, GRB Coordinates Network, 8611, 1
- . 2009, GRB Coordinates Network, 9553, 1
- Golenetskii, S., Aptekar, R., Frederiks, D., et al. 2010, GRB Coordinates Network, 11251, 1
- . 2014, GRB Coordinates Network, 16495, 1
- Gorbovskoy, E. S., Lipunova, G. V., Lipunov, V. M., et al. 2012, *MNRAS*, 421, 1874, doi: [10.1111/j.1365-2966.2012.20195.x](https://doi.org/10.1111/j.1365-2966.2012.20195.x)
- Guidorzi, C., Kobayashi, S., Perley, D. A., et al. 2011, *MNRAS*, 417, 2124, doi: [10.1111/j.1365-2966.2011.19394.x](https://doi.org/10.1111/j.1365-2966.2011.19394.x)
- H. E. S. S. Collaboration, Abdalla, H., Aharonian, F., et al. 2021, *Science*, 372, 1081, doi: [10.1126/science.abe8560](https://doi.org/10.1126/science.abe8560)
- Han, S., Li, X., Jiang, L., et al. 2022, *Universe*, 8, 248, doi: [10.3390/universe8040248](https://doi.org/10.3390/universe8040248)
- Harris, C. R., Millman, K. J., van der Walt, S. J., et al. 2020, *Nature*, 585, 357, doi: [10.1038/s41586-020-2649-2](https://doi.org/10.1038/s41586-020-2649-2)
- Hentunen, V.-P., & Nissinen, M. 2017, GRB Coordinates Network, 21113, 1
- Hu, Y. D., Oates, S. R., Lipunov, V. M., et al. 2019, *A&A*, 632, A100, doi: [10.1051/0004-6361/201834959](https://doi.org/10.1051/0004-6361/201834959)
- Huang, L.-Y., Wang, X.-G., Zheng, W., et al. 2018, *ApJ*, 859, 163, doi: [10.3847/1538-4357/aaba6e](https://doi.org/10.3847/1538-4357/aaba6e)
- Huang, X.-L., Liang, E.-W., Liu, R.-Y., Cheng, J.-G., & Wang, X.-Y. 2020, *ApJL*, 903, L26, doi: [10.3847/2041-8213/abc330](https://doi.org/10.3847/2041-8213/abc330)
- Huang, Y. F., Gou, L. J., Dai, Z. G., & Lu, T. 2000, *ApJ*, 543, 90, doi: [10.1086/317076](https://doi.org/10.1086/317076)
- Hunter, J. D. 2007, Computing in Science and Engineering, 9, 90, doi: [10.1109/MCSE.2007.55](https://doi.org/10.1109/MCSE.2007.55)
- Ioka, K. 2010, *Progress of Theoretical Physics*, 124, 667, doi: [10.1143/PTP.124.667](https://doi.org/10.1143/PTP.124.667)
- Ioka, K., Toma, K., Yamazaki, R., & Nakamura, T. 2006, *A&A*, 458, 7, doi: [10.1051/0004-6361:20064939](https://doi.org/10.1051/0004-6361:20064939)
- Isobe, T., Feigelson, E. D., Akritas, M. G., & Babu, G. J. 1990, *The Astrophysical Journal*, 364, 104, doi: [10.1086/169390](https://doi.org/10.1086/169390)
- Japelj, J., Kopač, D., Kobayashi, S., et al. 2014, *ApJ*, 785, 84, doi: [10.1088/0004-637X/785/2/84](https://doi.org/10.1088/0004-637X/785/2/84)
- Jin, Z. P., Xu, D., Covino, S., et al. 2009, *MNRAS*, 400, 1829, doi: [10.1111/j.1365-2966.2009.15555.x](https://doi.org/10.1111/j.1365-2966.2009.15555.x)
- Kang, Y., Liu, C., Zhu, J., & Shao, L. 2023, *Scientia Sinica Physica, Mechanica & Astronomica*, 53, 100014, doi: [10.1360/SSPMA-2022-0428](https://doi.org/10.1360/SSPMA-2022-0428)
- Kann, D. A., Klose, S., Zhang, B., et al. 2010, *ApJ*, 720, 1513, doi: [10.1088/0004-637X/720/2/1513](https://doi.org/10.1088/0004-637X/720/2/1513)
- Klužniak, W., & Ruderman, M. 1998, *ApJL*, 505, L113, doi: [10.1086/311622](https://doi.org/10.1086/311622)
- Kouveliotou, C., Meegan, C. A., Fishman, G. J., et al. 1993, *ApJL*, 413, L101, doi: [10.1086/186969](https://doi.org/10.1086/186969)
- Krimm, H. A., Yamaoka, K., Sugita, S., et al. 2009, *ApJ*, 704, 1405, doi: [10.1088/0004-637X/704/2/1405](https://doi.org/10.1088/0004-637X/704/2/1405)
- Kruehler, T., Schrey, F., Greiner, J., et al. 2008, GRB Coordinates Network, 8075, 1
- Krühler, T., Greiner, J., McBreen, S., et al. 2009a, *ApJ*, 697, 758, doi: [10.1088/0004-637X/697/1/758](https://doi.org/10.1088/0004-637X/697/1/758)
- Krühler, T., Greiner, J., Afonso, P., et al. 2009b, *A&A*, 508, 593, doi: [10.1051/0004-6361/200912649](https://doi.org/10.1051/0004-6361/200912649)
- Krühler, T., Ledoux, C., Fynbo, J. P. U., et al. 2013, *A&A*, 557, A18, doi: [10.1051/0004-6361/201321772](https://doi.org/10.1051/0004-6361/201321772)
- Kuin, N. P. M., Landsman, W., Page, M. J., et al. 2009, *MNRAS*, 395, L21, doi: [10.1111/j.1745-3933.2009.00632.x](https://doi.org/10.1111/j.1745-3933.2009.00632.x)
- Kumar, P. 1999, *ApJL*, 523, L113, doi: [10.1086/312265](https://doi.org/10.1086/312265)
- Kumar, P., Hernández, R. A., Bošnjak, Ž., & Barniol Duran, R. 2012, *MNRAS*, 427, L40, doi: [10.1111/j.1745-3933.2012.01341.x](https://doi.org/10.1111/j.1745-3933.2012.01341.x)
- Lan, L., Gao, H., Li, A., et al. 2023, *ApJL*, 949, L4, doi: [10.3847/2041-8213/accf93](https://doi.org/10.3847/2041-8213/accf93)
- Lemoine, M., & Pelletier, G. 2003, *ApJL*, 589, L73, doi: [10.1086/376353](https://doi.org/10.1086/376353)
- Liang, E. W., Dai, Z. G., & Wu, X. F. 2004, *ApJL*, 606, L29, doi: [10.1086/421047](https://doi.org/10.1086/421047)

- Liang, E.-W., Lin, T.-T., Lü, J., et al. 2015, ApJ, 813, 116, doi: [10.1088/0004-637X/813/2/116](https://doi.org/10.1088/0004-637X/813/2/116)
- Liang, E.-W., Yi, S.-X., Zhang, J., et al. 2010, ApJ, 725, 2209, doi: [10.1088/0004-637X/725/2/2209](https://doi.org/10.1088/0004-637X/725/2/2209)
- Liang, E.-W., Li, L., Gao, H., et al. 2013, ApJ, 774, 13, doi: [10.1088/0004-637X/774/1/13](https://doi.org/10.1088/0004-637X/774/1/13)
- Lithwick, Y., & Sari, R. 2001, ApJ, 555, 540, doi: [10.1086/321455](https://doi.org/10.1086/321455)
- Littlejohns, O. M., Willingale, R., O'Brien, P. T., et al. 2012, MNRAS, 421, 2692, doi: [10.1111/j.1365-2966.2012.20499.x](https://doi.org/10.1111/j.1365-2966.2012.20499.x)
- MAGIC Collaboration, Acciari, V. A., Ansoldi, S., et al. 2019a, Nature, 575, 455, doi: [10.1038/s41586-019-1750-x](https://doi.org/10.1038/s41586-019-1750-x)
- . 2019b, Nature, 575, 459, doi: [10.1038/s41586-019-1754-6](https://doi.org/10.1038/s41586-019-1754-6)
- Mazaeva, E., Antonyuk, K., Nikolenko, I., et al. 2017a, GRB Coordinates Network, 21169, 1
- Mazaeva, E., Pozanenko, A., Klunko, E., & Volnova, A. 2017b, GRB Coordinates Network, 21206, 1
- Mazaeva, E., Pozanenko, A., Kusakin, A., et al. 2017c, GRB Coordinates Network, 21208, 1
- McBreen, S. 2009, GRB Coordinates Network, 9535, 1
- Melandri, A., Kobayashi, S., Mundell, C. G., et al. 2010, ApJ, 723, 1331, doi: [10.1088/0004-637X/723/2/1331](https://doi.org/10.1088/0004-637X/723/2/1331)
- Mészáros, P. 2006, Reports on Progress in Physics, 69, 2259, doi: [10.1088/0034-4885/69/8/R01](https://doi.org/10.1088/0034-4885/69/8/R01)
- Meszaros, P., & Rees, M. J. 1993, ApJL, 418, L59, doi: [10.1086/187116](https://doi.org/10.1086/187116)
- Mészáros, P., & Rees, M. J. 1997, ApJ, 476, 232, doi: [10.1086/303625](https://doi.org/10.1086/303625)
- . 1999, MNRAS, 306, L39, doi: [10.1046/j.1365-8711.1999.02800.x](https://doi.org/10.1046/j.1365-8711.1999.02800.x)
- Molinari, E., Vergani, S. D., Malesani, D., et al. 2007, A&A, 469, L13, doi: [10.1051/0004-6361:20077388](https://doi.org/10.1051/0004-6361:20077388)
- Navia, L., Sironi, L., Ghisellini, G., Celotti, A., & Ghirlanda, G. 2013, MNRAS, 433, 2107, doi: [10.1093/mnras/stt872](https://doi.org/10.1093/mnras/stt872)
- Navia, L., Salvaterra, R., Ghirlanda, G., et al. 2012, MNRAS, 421, 1256, doi: [10.1111/j.1365-2966.2011.20394.x](https://doi.org/10.1111/j.1365-2966.2011.20394.x)
- Nousek, J. A., Kouveliotou, C., Grupe, D., et al. 2006, ApJ, 642, 389, doi: [10.1086/500724](https://doi.org/10.1086/500724)
- Paciesas, W. S., Meegan, C. A., Pendleton, G. N., et al. 1999, ApJS, 122, 465, doi: [10.1086/313224](https://doi.org/10.1086/313224)
- Page, K. L., Willingale, R., Bissaldi, E., et al. 2009, MNRAS, 400, 134, doi: [10.1111/j.1365-2966.2009.15462.x](https://doi.org/10.1111/j.1365-2966.2009.15462.x)
- Panaiteescu, A., Mészáros, P., Burrows, D., et al. 2006, MNRAS, 369, 2059, doi: [10.1111/j.1365-2966.2006.10453.x](https://doi.org/10.1111/j.1365-2966.2006.10453.x)
- Panaiteescu, A., Spada, M., & Mészáros, P. 1999, ApJL, 522, L105, doi: [10.1086/312230](https://doi.org/10.1086/312230)
- Piran, T. 1999, PhR, 314, 575, doi: [10.1016/S0370-1573\(98\)00127-6](https://doi.org/10.1016/S0370-1573(98)00127-6)
- Planck, C., Perovich, D. K., & Richter-Menge, J. 2016, in AGU Fall Meeting Abstracts, Vol. 2016, C21A–0664
- Poggiani, R., LIGO Scientific Collaboration, & Virgo Collaboration. 2019, in Frontier Research in Astrophysics - III. 28 May - 2 June 2018. Mondello (Palermo, 13, doi: [10.22323/1.331.0013](https://doi.org/10.22323/1.331.0013)
- Poggiani, R., LIGO Scientific Collaboration, & Virgo Collaboration. 2020, in Multifrequency Behaviour of High Energy Cosmic Sources - XIII. 3-8 June 2019. Palermo, 19, doi: [10.22323/1.362.0019](https://doi.org/10.22323/1.362.0019)
- Racusin, J. L., Karpov, S. V., Sokolowski, M., et al. 2008, Nature, 455, 183, doi: [10.1038/nature07270](https://doi.org/10.1038/nature07270)
- Rees, M. J., & Meszaros, P. 1992, MNRAS, 258, 41, doi: [10.1093/mnras/258.1.41P](https://doi.org/10.1093/mnras/258.1.41P)
- Ren, J., Wang, Y., & Dai, Z.-G. 2023, arXiv e-prints, arXiv:2310.15886, doi: [10.48550/arXiv.2310.15886](https://doi.org/10.48550/arXiv.2310.15886)
- Santana, R., Barniol Duran, R., & Kumar, P. 2014, ApJ, 785, 29, doi: [10.1088/0004-637X/785/1/29](https://doi.org/10.1088/0004-637X/785/1/29)
- Sari, R., & Esin, A. A. 2001, ApJ, 548, 787, doi: [10.1086/319003](https://doi.org/10.1086/319003)
- Sari, R., & Piran, T. 1995, ApJL, 455, L143, doi: [10.1086/309835](https://doi.org/10.1086/309835)
- . 1999a, ApJL, 517, L109, doi: [10.1086/312039](https://doi.org/10.1086/312039)
- . 1999b, ApJ, 520, 641, doi: [10.1086/307508](https://doi.org/10.1086/307508)
- Sari, R., Piran, T., & Narayan, R. 1998, ApJL, 497, L17, doi: [10.1086/311269](https://doi.org/10.1086/311269)
- Schlegel, D. J., Finkbeiner, D. P., & Davis, M. 1998, ApJ, 500, 525, doi: [10.1086/305772](https://doi.org/10.1086/305772)
- Stern, B. E., Tikhomirova, Y., Kompaneets, D., Svensson, R., & Poutanen, J. 2001, ApJ, 563, 80, doi: [10.1086/322295](https://doi.org/10.1086/322295)
- Suda, Y., Artero, M., Asano, K., et al. 2022, in 37th International Cosmic Ray Conference, 797, doi: [10.22323/1.395.0797](https://doi.org/10.22323/1.395.0797)
- Tavani, M. 1997, ApJL, 483, L87, doi: [10.1086/310751](https://doi.org/10.1086/310751)
- Thöne, C. C., Kann, D. A., Jóhannesson, G., et al. 2010, A&A, 523, A70, doi: [10.1051/0004-6361/200810340](https://doi.org/10.1051/0004-6361/200810340)
- Trotter, A., Haislip, J., LaCluyze, A., et al. 2013, GRB Coordinates Network, 14844, 1
- Trotter, A., Haislip, J., Reichart, D., et al. 2014, GRB Coordinates Network, 17210, 1
- Tsvetkova, A., Frederiks, D., Svinkin, D., et al. 2021, ApJ, 908, 83, doi: [10.3847/1538-4357/abd569](https://doi.org/10.3847/1538-4357/abd569)
- Ukwatta, T. N., Stamatikos, M., Dhuga, K. S., et al. 2010, ApJ, 711, 1073, doi: [10.1088/0004-637X/711/2/1073](https://doi.org/10.1088/0004-637X/711/2/1073)
- Usov, V. V. 1992, Nature, 357, 472, doi: [10.1038/357472a0](https://doi.org/10.1038/357472a0)
- Wang, X.-G., Zhang, B., Liang, E.-W., et al. 2015, ApJS, 219, 9, doi: [10.1088/0067-0049/219/1/9](https://doi.org/10.1088/0067-0049/219/1/9)

- Wang, Y., Aimuratov, Y., Moradi, R., et al. 2018, Mem. Soc. Astron. Italiana, 89, 293, doi: [10.48550/arXiv.1802.01693](https://doi.org/10.48550/arXiv.1802.01693)
- Waxman, E. 1997, ApJL, 485, L5, doi: [10.1086/310809](https://doi.org/10.1086/310809)
- Willingale, R., O'Brien, P. T., Goad, M. R., et al. 2007, arXiv e-prints, arXiv:0710.3727, doi: [10.48550/arXiv.0710.3727](https://doi.org/10.48550/arXiv.0710.3727)
- Woosley, S. E. 1993, ApJ, 405, 273, doi: [10.1086/172359](https://doi.org/10.1086/172359)
- Xin, L., Han, X., Li, H., et al. 2023, Nature Astronomy, 7, 724, doi: [10.1038/s41550-023-01930-0](https://doi.org/10.1038/s41550-023-01930-0)
- Xin, L. P., Wei, J. Y., Qiu, Y. L., et al. 2017, GRB Coordinates Network, 20576, 1
- Xin, L.-P., Zhong, S.-Q., Liang, E.-W., et al. 2018, ApJ, 860, 8, doi: [10.3847/1538-4357/aabf3d](https://doi.org/10.3847/1538-4357/aabf3d)
- Yi, S.-X., Wu, X.-F., Zou, Y.-C., & Dai, Z.-G. 2020, ApJ, 895, 94, doi: [10.3847/1538-4357/ab8a53](https://doi.org/10.3847/1538-4357/ab8a53)
- Yost, S. A., Swan, H. F., Rykoff, E. S., et al. 2007, ApJ, 657, 925, doi: [10.1086/510896](https://doi.org/10.1086/510896)
- Yuan, F., Schady, P., Racusin, J. L., et al. 2010, ApJ, 711, 870, doi: [10.1088/0004-637X/711/2/870](https://doi.org/10.1088/0004-637X/711/2/870)
- Zhang, B. 2011, Comptes Rendus Physique, 12, 206, doi: [10.1016/j.crhy.2011.03.004](https://doi.org/10.1016/j.crhy.2011.03.004)
- . 2018, The Physics of Gamma-Ray Bursts, doi: [10.1017/9781139226530](https://doi.org/10.1017/9781139226530)
- Zhang, B., Fan, Y. Z., Dyks, J., et al. 2006, ApJ, 642, 354, doi: [10.1086/500723](https://doi.org/10.1086/500723)
- Zhang, B., & Mészáros, P. 2002, ApJ, 566, 712, doi: [10.1086/338247](https://doi.org/10.1086/338247)
- . 2004, International Journal of Modern Physics A, 19, 2385, doi: [10.1142/S0217751X0401746X](https://doi.org/10.1142/S0217751X0401746X)
- Zhang, B., & Pe'er, A. 2009, ApJL, 700, L65, doi: [10.1088/0004-637X/700/2/L65](https://doi.org/10.1088/0004-637X/700/2/L65)
- Zhang, B., & Yan, H. 2011, ApJ, 726, 90, doi: [10.1088/0004-637X/726/2/90](https://doi.org/10.1088/0004-637X/726/2/90)
- Zhang, B., Liang, E., Page, K. L., et al. 2007, ApJ, 655, 989, doi: [10.1086/510110](https://doi.org/10.1086/510110)
- Zhang, L.-L., Ren, J., Huang, X.-L., et al. 2021, ApJ, 917, 95, doi: [10.3847/1538-4357/ac0c7f](https://doi.org/10.3847/1538-4357/ac0c7f)
- Zhang, L.-L., Ren, J., Wang, Y., & Liang, E.-W. 2023, ApJ, 952, 127, doi: [10.3847/1538-4357/acd190](https://doi.org/10.3847/1538-4357/acd190)
- Zhang, L.-L., Xin, L.-P., Wang, J., et al. 2022, ApJ, 941, 63, doi: [10.3847/1538-4357/aca08f](https://doi.org/10.3847/1538-4357/aca08f)
- Zitouni, H., Guessoum, N., Azzam, W. J., & Benturki, Y. 2020, Ap&SS, 365, 177, doi: [10.1007/s10509-020-03893-4](https://doi.org/10.1007/s10509-020-03893-4)

Table 1. The selected time intervals of the optical and X-ray afterglow light curves for our fits with the FS model

GRBs	X-ray afterglows	Optical afterglows
	(s)	(s)
GRB 050820A	$4.68 \times 10^3 - 3.69 \times 10^6$	$230 - 6.63 \times 10^5$
GRB 050922C	$1.17 \times 10^2 - 3.56 \times 10^5$	$7.45 \times 10^2 - 6.06 \times 10^5$
GRB 051109A	$3.56 \times 10^3 - 1.50 \times 10^6$	$39.7 - 1.04 \times 10^6$
GRB 051111	$5.63 \times 10^3 - 4.76 \times 10^4$	$31.9 - 7587$
GRB 060418	$342.22 - 5.37 \times 10^5$	$76 - 7659$
GRB 060526	$885.34 - 3.11 \times 10^5$	$593.10 - 6.38 \times 10^5$
GRB 070318	$637.99 - 7.88 \times 10^5$	$60.72 - 8.74 \times 10^4$
GRB 070411	$499.28 - 7.10 \times 10^5$	$183.47 - 5.17 \times 10^5$
GRB 071010A	$3.45 \times 10^4 - 4.73 \times 10^5$	$320.90 - 5.07 \times 10^5$
GRB 071031	$6.13 \times 10^3 - 3.04 \times 10^5$	$287.30 - 2.57 \times 10^4$
GRB 071112C	$1.25 \times 10^4 - 3.56 \times 10^5$	$131.99 - 6.96 \times 10^4$
GRB 080310	$1.03 \times 10^3 - 6.86 \times 10^5$	$298.3 - 1.24 \times 10^5$
GRB 080603A	$1.05 \times 10^4 - 6.02 \times 10^5$	$105 - 3.50 \times 10^5$
GRB 080710	$3.19 \times 10^3 - 5.56 \times 10^5$	$416.9 - 2.67 \times 10^5$
GRB 080810	$304.25 - 3.79 \times 10^5$	$38 - 4.98 \times 10^5$
GRB 081008	$488.38 - 2.99 \times 10^5$	$108.82 - 1.85 \times 10^5$
GRB 081109A	$338.56 - 4.76 \times 10^5$	$168.9 - 6.66 \times 10^4$
GRB 081203A	$150.99 - 3.41 \times 10^5$	$28.48 - 5.71 \times 10^3$
GRB 090313	$2.68 \times 10^4 - 7.17 \times 10^5$	$204.6 - 3.75 \times 10^5$
GRB 090618	$311.90 - 2.90 \times 10^6$	$76 - 7.26 \times 10^4$
GRB 100906A	$206.11 - 2.02 \times 10^5$	$51.35 - 1.09 \times 10^4$
GRB 120729A	$59.87 - 4.25 \times 10^4$	$30.4 - 5.44 \times 10^4$
GRB 120815A	$2.74 \times 10^3 - 4.88 \times 10^4$	$169 - 11053$
GRB 130610A	$324.9 - 2.28 \times 10^5$	$122 - 2.25 \times 10^3$
GRB 140629A	$82.67 - 9.16 \times 10^4$	$71.80 - 35347$
GRB 141221A	$88.52 - 137.42; 3.90 \times 10^3 - 1.90 \times 10^5$	$68.7 - 1600$
GRB 160203A	$318.85 - 1.53 \times 10^5$	$258 - 3680$
GRB 170202A	$433.86 - 3.42 \times 10^5$	$68 - 9309$
GRB 170519A	$467.91 - 1.67 \times 10^5$	$1119 - 2.99 \times 10^5$
GRB 181110A	$422.88 - 1.15 \times 10^5$	$720 - 5.58 \times 10^4$

Table 2. The prior range of model parameters of FS.

Parameter	$\log E_{k,\text{iso}}/\text{erg}$	$\log \Gamma_0$	$\log n/\text{cm}^{-3}$	p	$\log \theta_j$	$\log \epsilon_e$	$\log \epsilon_B$
Range	[52.5, 56.5]	[1, 3.5]	[-3, 3]	[2.05, 3]	[-2, -0.5]	[-3.3, -0.3]	[-8, -2]

Table 3. The derived model parameters from our fits to the optical and X-ray afterglow light curves with the standard external shock model, along with several inferred quantities such as prompt and afterglow properties.

GRB(Band) Ref	z	$\log(E_{\text{K,iso}})$	$\log(n)$	$\log(\Gamma_0)$	p	$\log(\theta_j/\text{rad})$	$\log(\epsilon_e)$	$\log(e_B)$	$E_{\gamma,\text{iso}}$	$L_{\text{p,iso}}$	$E_{\text{p,z}}$	η_γ	B_0	R_{dec}
		(erg)	(cm $^{-3}$)			(rad)		(erg)	(10 52 erg/s)			(%)	(Gs)	(10 17 cm)
GRB 050820A(R)(1)	2.612	55.97 $^{+0.02}_{-0.02}$	-2.99 $^{+0.01}_{-0.01}$	2.84 $^{+0.01}_{-0.01}$	2.22 $^{+0.01}_{-0.01}$	-1.59 $^{+0.01}_{-0.01}$	-2.25 $^{+0.01}_{-0.01}$	-3.28 $^{+0.02}_{-0.01}$	8.30e53	5.78 $^{+3.05}_{-3.05}$	978.85	1.03	0.20	35.68
GRB 050922C(R)(2)	2.198	54.05 $^{+0.06}_{-0.06}$	-0.76 $^{+0.18}_{-0.13}$	2.53 $^{+0.02}_{-0.02}$	2.58 $^{+0.02}_{-0.02}$	-1.30 $^{+0.02}_{-0.02}$	-1.47 $^{+0.05}_{-0.04}$	-3.82 $^{+0.15}_{-0.15}$	8.10e52	5.17 $^{+28.00}_{-28.00}$	457.31	6.73	0.68	2.38
GRB 051109A(R)(3)	2.346	55.99 $^{+0.01}_{-0.01}$	1.74 $^{+0.04}_{-0.04}$	2.60 $^{+0.01}_{-0.01}$	2.05 $^{+0.01}_{-0.01}$	-1.39 $^{+0.01}_{-0.01}$	-1.87 $^{+0.02}_{-0.02}$	-6.96 $^{+0.05}_{-0.03}$	5.00e52	10.11 $^{+9.14}_{-9.14}$	538.71	0.05	0.38	1.39
GRB 051111(R)(4)	1.55	56.09 $^{+0.18}_{-0.18}$	1.47 $^{+0.24}_{-0.24}$	2.80 $^{+0.01}_{-0.01}$	2.05 $^{+0.01}_{-0.01}$	-1.91 $^{+0.01}_{-0.01}$	-3.11 $^{+0.31}_{-0.31}$	-5.37 $^{+0.31}_{-0.30}$	6.30e52	1.55 $^{+0.61}_{-0.61}$	1139.85	0.05	2.75	2.38
GRB 060418(H)(5)	1.49	55.75 $^{+0.25}_{-0.25}$	-2.72 $^{+0.22}_{-0.22}$	2.94 $^{+0.03}_{-0.03}$	2.41 $^{+0.06}_{-0.06}$	-1.97 $^{+0.03}_{-0.03}$	-2.92 $^{+0.14}_{-0.14}$	-2.61 $^{+0.33}_{-0.33}$	9.00e52	5.75 $^{+3.18}_{-3.18}$	572.70	0.16	0.73	21.01
GRB 060526(Re)(6)	3.21	52.66 $^{+0.02}_{-0.02}$	2.84 $^{+0.16}_{-0.14}$	1.58 $^{+0.02}_{-0.02}$	2.05 $^{+0.01}_{-0.01}$	-0.76 $^{+0.02}_{-0.02}$	-0.90 $^{+0.02}_{-0.02}$	-3.10 $^{+0.13}_{-0.13}$	—	5.04 $^{+4.05}_{-4.05}$	164.19	—	10.97	0.22
GRB 070318(V)(7)	0.84	53.69 $^{+0.07}_{-0.07}$	2.33 $^{+0.22}_{-0.22}$	1.98 $^{+0.02}_{-0.02}$	2.07 $^{+0.02}_{-0.02}$	-0.50 $^{+0.02}_{-0.02}$	-0.53 $^{+0.02}_{-0.02}$	-5.52 $^{+0.33}_{-0.35}$	1.45e52	0.18 $^{+0.05}_{-0.05}$	671.60	6.51	0.94	0.39
GRB 070411(R)(8)	2.95	54.75 $^{+0.05}_{-0.05}$	-2.40 $^{+0.76}_{-0.43}$	2.72 $^{+0.05}_{-0.05}$	2.26 $^{+0.02}_{-0.02}$	—	-2.02 $^{+0.12}_{-0.12}$	-2.74 $^{+0.37}_{-0.37}$	—	1.77 $^{+0.51}_{-0.51}$	474	—	0.55	10.69
GRB 071010A(R)(9)	0.98	54.44 $^{+0.08}_{-0.08}$	-0.28 $^{+0.26}_{-0.26}$	2.18 $^{+0.03}_{-0.03}$	2.05 $^{+0.01}_{-0.01}$	-1.23 $^{+0.03}_{-0.03}$	-2.25 $^{+0.07}_{-0.07}$	-3.18 $^{+0.20}_{-0.20}$	—	0.03 $^{+0.02}_{-0.02}$	69.3	—	1.17	3.71
GRB 071031(r')(10)	2.69	54.46 $^{+0.06}_{-0.06}$	0.30 $^{+0.26}_{-0.27}$	2.14 $^{+0.03}_{-0.03}$	2.05 $^{+0.01}_{-0.01}$	-1.22 $^{+0.03}_{-0.03}$	-2.22 $^{+0.09}_{-0.09}$	-3.08 $^{+0.20}_{-0.20}$	—	0.14 $^{+0.04}_{-0.04}$	110.7	—	2.19	2.62
GRB 071112C(R)(11)	0.82	53.49 $^{+0.10}_{-0.14}$	-0.85 $^{+0.25}_{-0.25}$	2.46 $^{+0.03}_{-0.03}$	2.12 $^{+0.03}_{-0.03}$	-1.33 $^{+0.04}_{-0.04}$	-1.37 $^{+0.12}_{-0.12}$	-4.03 $^{+0.22}_{-0.22}$	—	8.71 $^{+6.62}_{-6.62}$	—	0.41	1.84	—
GRB 080310(R)(12)	2.42	53.87 $^{+0.04}_{-0.04}$	1.01 $^{+0.15}_{-0.15}$	2.34 $^{+0.03}_{-0.03}$	2.10 $^{+0.01}_{-0.01}$	-1.03 $^{+0.01}_{-0.01}$	-0.63 $^{+0.03}_{-0.03}$	-4.60 $^{+0.24}_{-0.24}$	—	0.31 $^{+0.09}_{-0.09}$	257.87	—	1.36	0.71
GRB 080603A(R)(13)	2.69	54.87 $^{+0.08}_{-0.09}$	-0.93 $^{+0.30}_{-0.30}$	2.53 $^{+0.02}_{-0.02}$	2.41 $^{+0.01}_{-0.01}$	-1.44 $^{+0.05}_{-0.05}$	-0.58 $^{+0.03}_{-0.03}$	-6.38 $^{+0.17}_{-0.17}$	—	160	—	0.03	5.08	—
GRB 080710(r')(14)	0.85	52.94 $^{+0.15}_{-0.15}$	-1.25 $^{+0.16}_{-0.19}$	2.00 $^{+0.03}_{-0.03}$	2.45 $^{+0.11}_{-0.11}$	-1.29 $^{+0.02}_{-0.02}$	-1.15 $^{+0.04}_{-0.04}$	-2.04 $^{+0.03}_{-0.03}$	—	0.04 $^{+0.01}_{-0.01}$	200	—	0.88	3.33
GRB 080810(R)(15)	3.35	55.50 $^{+0.01}_{-0.01}$	0.07 $^{+0.06}_{-0.06}$	2.78 $^{+0.01}_{-0.01}$	2.50 $^{+0.01}_{-0.01}$	-1.27 $^{+0.01}_{-0.01}$	-2.37 $^{+0.01}_{-0.01}$	-3.98 $^{+0.05}_{-0.05}$	3.00e53	7.84	2475.15	0.94	2.60	2.60
GRB 081008(r')(16)	1.967	55.35 $^{+0.05}_{-0.05}$	-2.94 $^{+0.04}_{-0.04}$	2.86 $^{+0.01}_{-0.01}$	2.21 $^{+0.01}_{-0.01}$	-1.96 $^{+0.01}_{-0.01}$	-2.20 $^{+0.01}_{-0.01}$	-3.70 $^{+0.09}_{-0.09}$	6.30e52	0.92	261.7	0.60	0.13	20.69
GRB 081109A(H)(17)	0.9787	55.38 $^{+0.09}_{-0.09}$	-3.51 $^{+0.25}_{-0.16}$	2.81 $^{+0.03}_{-0.03}$	2.06 $^{+0.01}_{-0.01}$	-1.93 $^{+0.03}_{-0.03}$	-3.08 $^{+0.17}_{-0.17}$	-2.12 $^{+0.17}_{-0.17}$	5.00e52	0.43	474.89	0.21	0.38	35.40
GRB 081203A(U)(18)	2.05	54.92 $^{+0.15}_{-0.15}$	1.73 $^{+0.11}_{-0.14}$	2.33 $^{+0.02}_{-0.02}$	2.57 $^{+0.01}_{-0.01}$	-1.39 $^{+0.01}_{-0.01}$	-1.38 $^{+0.03}_{-0.03}$	-6.10 $^{+0.23}_{-0.23}$	3.50e53	2.82 $^{+0.19}_{-0.19}$	1762.9	4.04	0.54	0.94
GRB 090313(r')(19)	3.375	55.31 $^{+0.11}_{-0.11}$	-2.19 $^{+0.24}_{-0.19}$	2.59 $^{+0.03}_{-0.03}$	2.07 $^{+0.01}_{-0.01}$	-1.73 $^{+0.03}_{-0.03}$	-2.15 $^{+0.16}_{-0.16}$	-2.24 $^{+0.15}_{-0.15}$	—	0.36 $^{+0.31}_{-0.31}$	—	—	—	17.08
GRB 090618(R)(20)	0.54	55.45 $^{+0.07}_{-0.07}$	-2.05 $^{+0.16}_{-0.16}$	2.74 $^{+0.02}_{-0.02}$	2.05 $^{+0.01}_{-0.01}$	-1.75 $^{+0.02}_{-0.02}$	-2.63 $^{+0.07}_{-0.07}$	-3.38 $^{+0.11}_{-0.11}$	2.00e53	1.91 $^{+0.22}_{-0.22}$	338.8	0.71	0.41	13.56
GRB 100906A(V)(21)	1.727	55.38 $^{+0.01}_{-0.01}$	0.20 $^{+0.06}_{-0.06}$	2.56 $^{+0.02}_{-0.02}$	2.51 $^{+0.01}_{-0.01}$	-1.50 $^{+0.01}_{-0.01}$	-1.97 $^{+0.01}_{-0.01}$	-5.34 $^{+0.05}_{-0.05}$	2.20e53	1.51 $^{+0.07}_{-0.07}$	387.23	0.69	0.38	3.30
GRB 120729A(R)(22)	0.8	55.38 $^{+0.37}_{-0.38}$	0.59 $^{+0.31}_{-0.31}$	2.61 $^{+0.01}_{-0.01}$	2.36 $^{+0.01}_{-0.01}$	-1.78 $^{+0.01}_{-0.01}$	-2.90 $^{+0.23}_{-0.23}$	-4.89 $^{+0.31}_{-0.31}$	2.30e52	—	—	0.10	1.12	2.07
GRB 120815A(r')(23)	2.358	53.88 $^{+0.02}_{-0.02}$	-2.61 $^{+0.27}_{-0.23}$	2.99 $^{+0.01}_{-0.01}$	2.07 $^{+0.01}_{-0.01}$	-1.96 $^{+0.05}_{-0.05}$	-2.44 $^{+0.17}_{-0.17}$	-3.76 $^{+0.38}_{-0.38}$	—	—	—	1.14	4.26	—
GRB 130610A(I)(24)	2.092	55.28 $^{+0.16}_{-0.16}$	-1.94 $^{+0.10}_{-0.05}$	2.72 $^{+0.02}_{-0.03}$	2.34 $^{+0.01}_{-0.01}$	-1.72 $^{+0.04}_{-0.03}$	-2.07 $^{+0.10}_{-0.10}$	-4.93 $^{+0.53}_{-0.53}$	6.18e52	1.08	911.83	0.32	0.07	11.28
GRB 140629A(R)(25)	2.275	56.00 $^{+0.01}_{-0.01}$	0.67 $^{+0.06}_{-0.06}$	2.55 $^{+0.01}_{-0.01}$	2.59 $^{+0.01}_{-0.01}$	-1.58 $^{+0.01}_{-0.01}$	-2.25 $^{+0.04}_{-0.04}$	-5.86 $^{+0.40}_{-0.40}$	4.40e52	1.86 $^{+0.69}_{-0.73}$	281.65	0.04	0.35	3.43
GRB 141221A(I)(26)	1.45	55.48 $^{+0.01}_{-0.01}$	-2.85 $^{+0.11}_{-0.11}$	2.89 $^{+0.01}_{-0.01}$	2.37 $^{+0.01}_{-0.01}$	—	-2.43 $^{+0.03}_{-0.03}$	-3.83 $^{+0.11}_{-0.11}$	6.99e52	0.77	328.13	0.23	0.14	20.37
GRB 160203A(I)(27)	3.52	55.16 $^{+0.23}_{-0.30}$	1.35 $^{+0.49}_{-0.47}$	2.23 $^{+0.04}_{-0.04}$	2.07 $^{+0.02}_{-0.02}$	-1.37 $^{+0.04}_{-0.04}$	-2.63 $^{+0.33}_{-0.25}$	-4.31 $^{+0.41}_{-0.41}$	1.20e53	—	—	0.82	2.19	1.75
GRB 170702A(R)(28)	3.645	55.50 $^{+0.01}_{-0.01}$	-2.77 $^{+0.08}_{-0.08}$	2.90 $^{+0.01}_{-0.01}$	2.22 $^{+0.01}_{-0.01}$	-1.68 $^{+0.04}_{-0.04}$	-2.23 $^{+0.01}_{-0.01}$	-3.66 $^{+0.06}_{-0.05}$	1.70e53	17.40 $^{+18.00}_{-14.40}$	1147.32	0.54	0.19	19.16
GRB 170519A(R)(29)	3.52	53.74 $^{+0.03}_{-0.04}$	2.93 $^{+0.05}_{-0.05}$	1.52 $^{+0.01}_{-0.01}$	2.07 $^{+0.01}_{-0.01}$	-0.68 $^{+0.01}_{-0.01}$	-0.42 $^{+0.04}_{-0.04}$	-4.96 $^{+0.11}_{-0.08}$	—	—	—	1.24	0.52	—
GRB 1811110A(R)(30)	3.52	55.02 $^{+0.06}_{-0.04}$	2.99 $^{+0.01}_{-0.02}$	1.81 $^{+0.01}_{-0.01}$	2.06 $^{+0.01}_{-0.01}$	—	-1.04 $^{+0.05}_{-0.06}$	-4.95 $^{+0.06}_{-0.06}$	1.34e53	0.48 $^{+0.21}_{-0.61}$	132.44	1.26	2.63	0.85

References— (1) Cenko et al. (2007); Willingale et al. (2005); Golenetskii et al. (2006); Panaitescu et al. (2005b); Yost et al. (2007); Willingale et al. (2007); Thöne et al. (2007); Butler et al. (2006); Beskin et al. (2015); (2) Krimm et al. (2009); (3) Golenetskii et al. (2010); (4) Butler et al. (2007); Ferrero et al. (2007); Covino et al. (2008); Beskin et al. (2010); (5) Molinari et al. (2009); (6) Willingale et al. (2007); Thöne et al. (2007); (7) Beskin et al. (2015); (8) Butler et al. (2008); Willingale et al. (2008); Covino et al. (2008); Beskin et al. (2009); (9) Covino et al. (2015); (10) Kruhler et al. (2015); (11) Kruehler et al. (2010); (12) Kann et al. et al. (2010); (13) Littlejohns et al. (2010); (14) Kruhler et al. (2009b); Beskin et al. (2010); (15) Page et al. (2009); Melandri et al. (2010); (16) Yuan et al. (2010); (17) Jin et al. (2010); (18) Golenetskii et al. (2009); (19) McBreen (2009); (20) McBreen (2015); (21) Golenetskii et al. (2011); (22) Golenetskii et al. (2015); (23) Kruhler et al. (2014); Huang et al. (2018); (24) Trotter et al. (2013); (25) Golenetskii et al. (2013); (26) Trotter et al. (2020); (27) Zitouni et al. (2022); (28) Crisp et al. (2021); (29) Golenetskii et al. (2015); (30) Zitouni et al. (2017a,b,c); (31) Mazaeva et al. (2017); (32) Golenetskii et al. (2010); (33) Golenetskii et al. (2006); (34) Golenetskii et al. (2009); (35) Golenetskii et al. (2010); (36) Willingale et al. (2007); (37) Willingale et al. (2007); (38) Golenetskii et al. (2010); (39) Covino et al. (2015); (40) Covino et al. (2012); (41) Beskin et al. (2012); (42) Beskin et al. (2010); (43) Covino et al. (2010); (44) Covino et al. (2012); (45) Covino et al. (2012); (46) Willingale et al. (2007); (47) Willingale et al. (2007); (48) Golenetskii et al. (2010); (49) Covino et al. (2015); (50) Covino et al. (2012); (51) Beskin et al. (2012); (52) Beskin et al. (2010); (53) Covino et al. (2010); (54) Covino et al. (2012); (55) Covino et al. (2012); (56) Covino et al. (2012); (57) Covino et al. (2012); (58) Covino et al. (2012); (59) Covino et al. (2012); (60) Covino et al. (2012); (61) Covino et al. (2012); (62) Covino et al. (2012); (63) Covino et al. (2012); (64) Covino et al. (2012); (65) Covino et al. (2012); (66) Covino et al. (2012); (67) Covino et al. (2012); (68) Covino et al. (2012); (69) Covino et al. (2012); (70) Covino et al. (2012); (71) Covino et al. (2012); (72) Covino et al. (2012); (73) Covino et al. (2012); (74) Covino et al. (2012); (75) Covino et al. (2012); (76) Covino et al. (2012); (77) Covino et al. (2012); (78) Covino et al. (2012); (79) Covino et al. (2012); (80) Covino et al. (2012); (81) Covino et al. (2012); (82) Covino et al. (2012); (83) Covino et al. (2012); (84) Covino et al. (2012); (85) Covino et al. (2012); (86) Covino et al. (2012); (87) Covino et al. (2012); (88) Covino et al. (2012); (89) Covino et al. (2012); (90) Covino et al. (2012); (91) Covino et al. (2012); (92) Covino et al. (2012); (93) Covino et al. (2012); (94) Covino et al. (2012); (95) Covino et al. (2012); (96) Covino et al. (2012); (97) Covino et al. (2012); (98) Covino et al. (2012); (99) Covino et al. (2012); (100) Covino et al. (2012); (101) Covino et al. (2012); (102) Covino et al. (2012); (103) Covino et al. (2012); (104) Covino et al. (2012); (105) Covino et al. (2012); (106) Covino et al. (2012); (107) Covino et al. (2012); (108) Covino et al. (2012); (109) Covino et al. (2012); (110) Covino et al. (2012); (111) Covino et al. (2012); (112) Covino et al. (2012); (113) Covino et al. (2012); (114) Covino et

Table 4. The distributions and our log-normal/bimodal fits of the jet properties for the bursts in our sample.

Parameter	Range	Median	Average	Normality/Bimodality ^a	Adj. R^2
$\log E_{k,\text{iso}}/\text{erg}$	[52.5, 56.5]	55.22	54.70	$N_1(53.81, 0.28)$ $N_2(55.34, 0.45)$	0.90
$\log E_{\gamma,\text{iso}}/\text{erg}$	[52, 54]	52.91	53.07	$N(52.96, 0.37)$	0.92
$\log \theta_j/\text{rad}$	[-2, 0.5]	-1.47	-1.24	$N(-1.51, 0.27)$	0.95
$\log E_{k,j}/\text{erg}$	[50, 53]	51.71	51.33	$N(51.78, 0.54)$	0.98
$\log E_{\gamma,j}/\text{erg}$	[48, 51.5]	49.57	49.25	$N(49.47, 0.87)$	0.99
$\log \eta_\gamma/\%$	[-1.4, 1]	-0.27	-0.10	$N(-0.38, 0.76)$	0.93
$\log \Gamma_0$	[1, 3]	2.58	2.57	$N(2.63, 0.27)$	0.83
$\log(M_{\text{fb}}/M_\odot)$	[-6.5, -3.5]	-5.08	-5.50	$N(-5.00, 0.75)$	0.95
$\log n/\text{cm}^{-3}$	[-3, 3]	-0.35	-0.08	$N_1(-2.51, 0.50)$ $N_2(1.00, 1.34)$	0.88
$\log R_{\text{dec}}/10^{17}\text{cm}$	[-1, 2]	0.52	0.45	$N(0.59, 0.56)$	0.99
$\log \epsilon_B$	[-7, -1.5]	-3.91	-4.40	$N(-4.09, 1.90)$	0.91
$\log \epsilon_e$	[-3.5, -0.3]	-2.11	-2.20	$N_1(-2.39, 0.36)$ $N_2(-0.95, 0.39)$	0.88
$\log \sigma_B$	[-5.5, 0.5]	-1.84	-2.17	$N_1(-4.2, 1.06)$ $N_2(-1.30, 0.68)$	0.89
$\log B_0/\text{Gs}$	[-1.6, 1.2]	-0.15	-0.06	$N(-0.17, 0.54)$	0.99

^a The results of our fits with a normal function $N(x_c, \sigma)$ or bimodal function $N_1(x_{c,1}, \sigma_1) + N_2(x_{c,2}, \sigma_2)$.

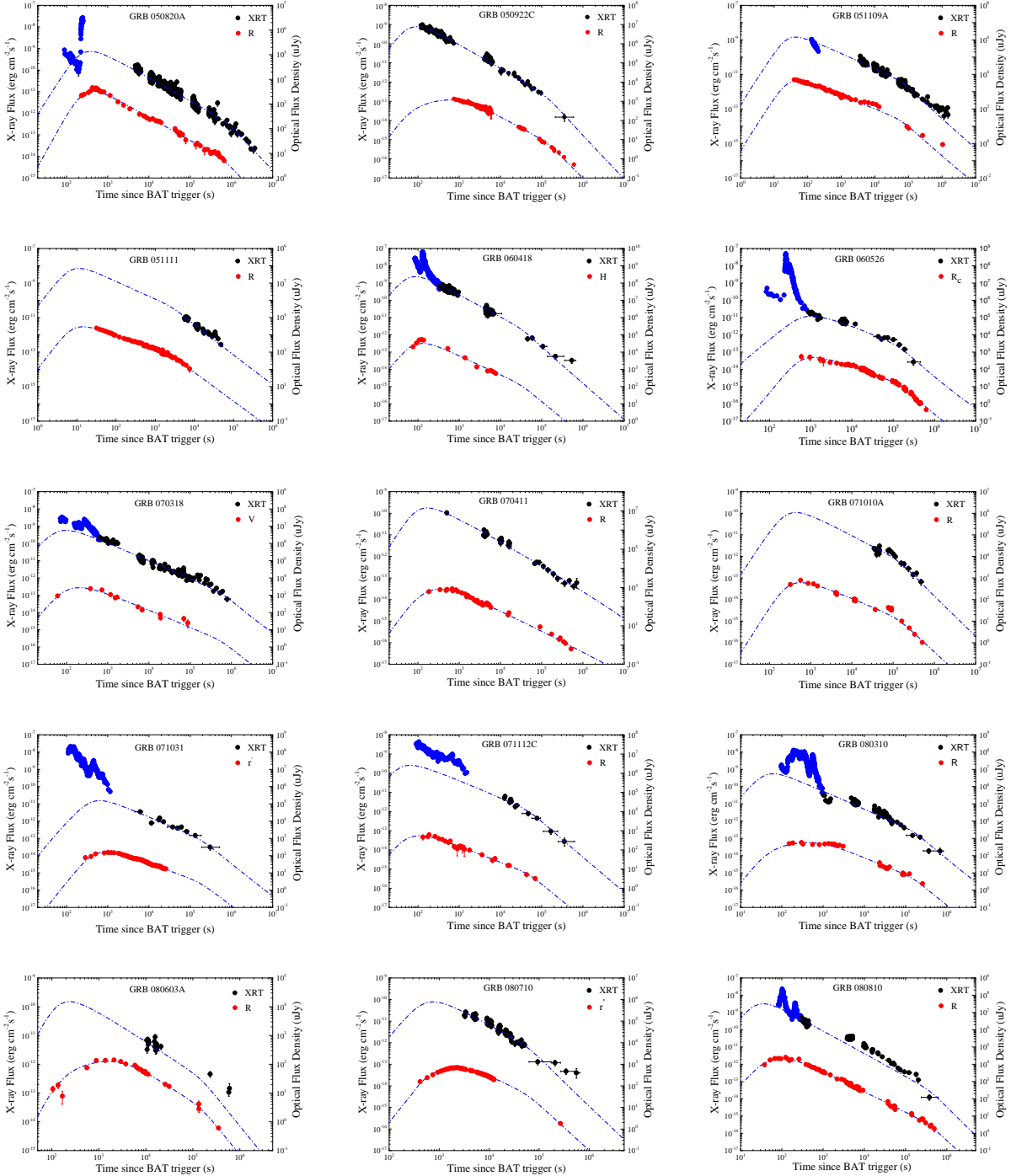
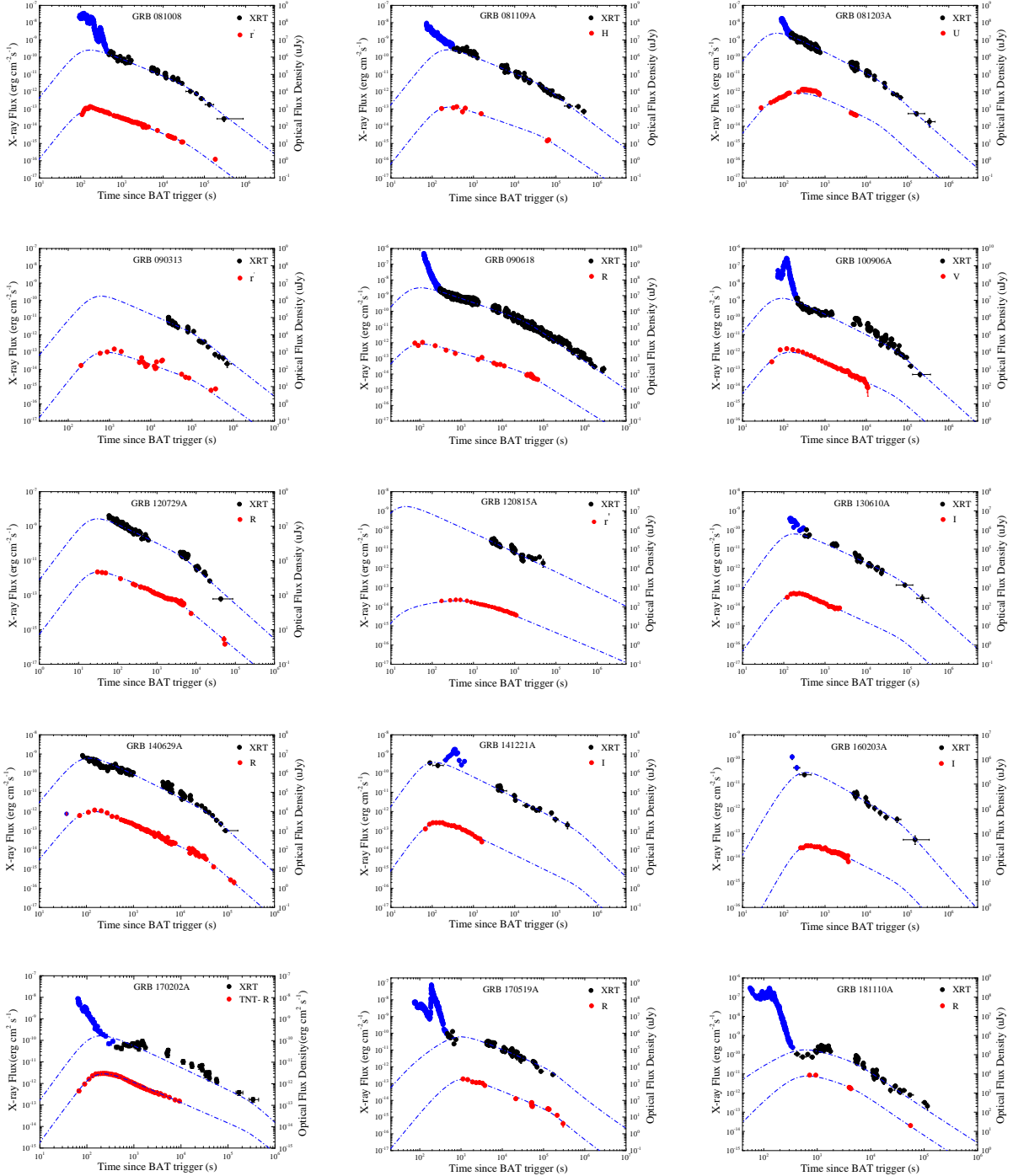


Figure 1. Optical and X-ray afterglow light curves (data points) of the bursts in our sample and our theoretical fits (dashed-dotted lines) with the standard FS model by utilizing the `pymultinest` package.



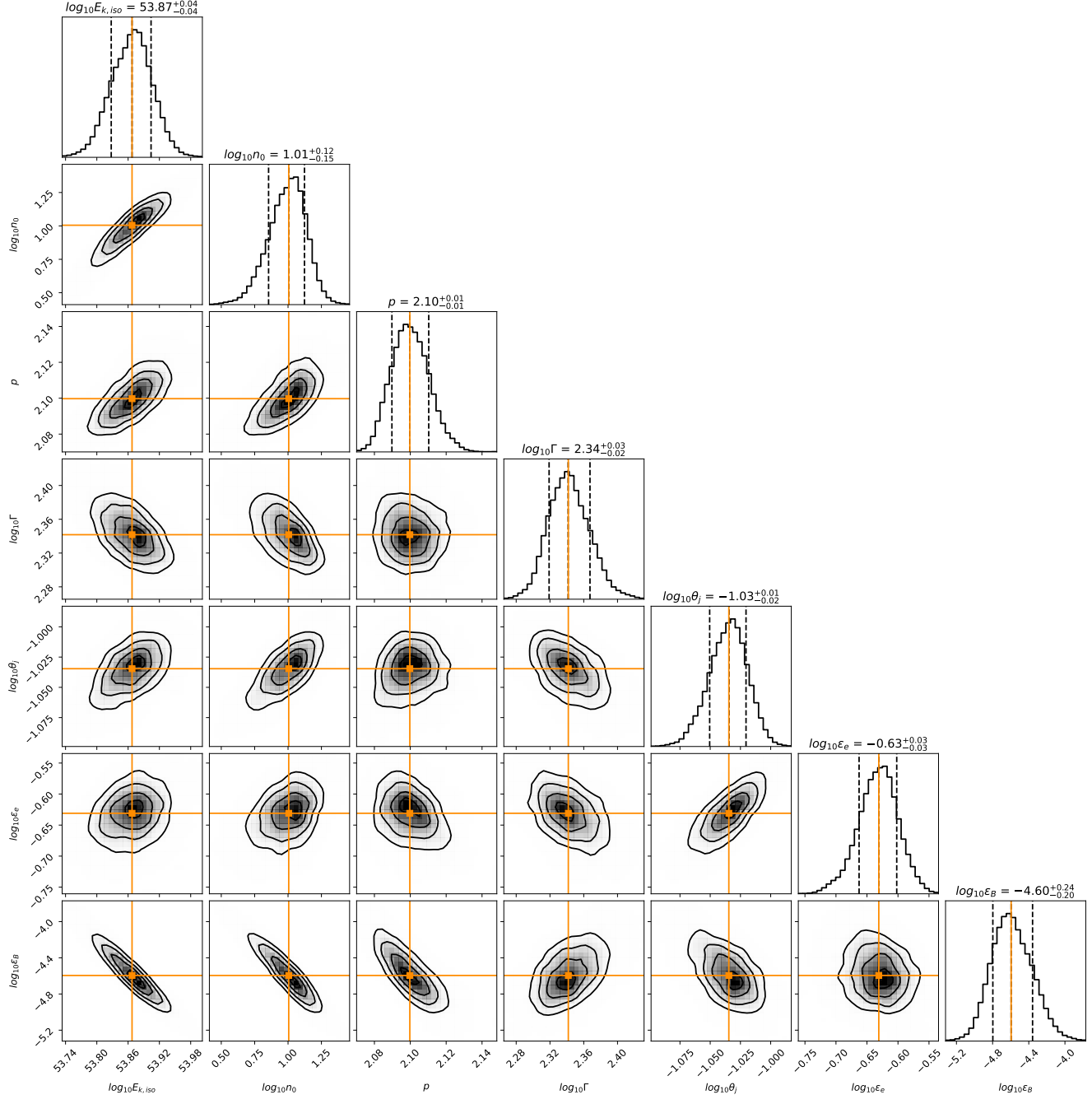


Figure 2. Posterior probability distributions of the model parameters of GRB 080310 derived from our fit with the `pymultinest` package. The vertical dashed lines mark the 1σ confidence level regions centering at the medians of the probability distributions.

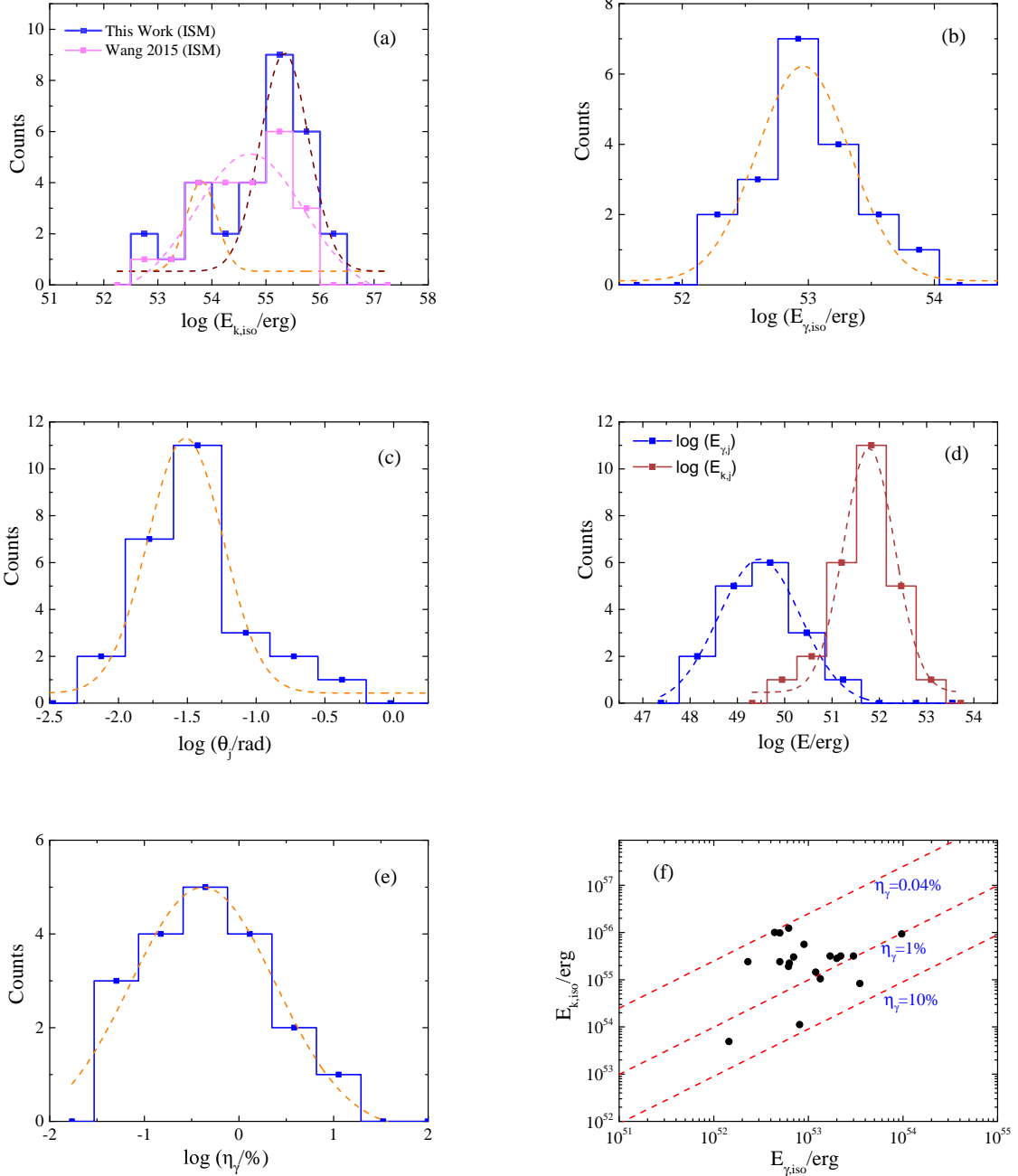


Figure 3. Distributions of $\log(E_{k,\text{iso}})$, $\log(E_{\gamma,\text{iso}})$, $\log(\theta_j)$, $\log(E_{k,j})$, $\log(E_{\gamma,j})$, and $\log(\eta_\gamma)$ as well as $E_{k,\text{iso}}$ as a function of $E_{\gamma,\text{iso}}$ for the bursts in our sample. The dashed curves are the best fit with a Gaussian function or a two-Gaussian function model in panels (a)-(e). The $\log E_{k,\text{iso}}$ distribution taken from Wang et al. (2015) is also shown with a magenta curve in panel (a) for comparison. The red dashed lines mark the line for $\eta_\gamma = 0.04\%$, 0.1% , and 10% in panel (f).

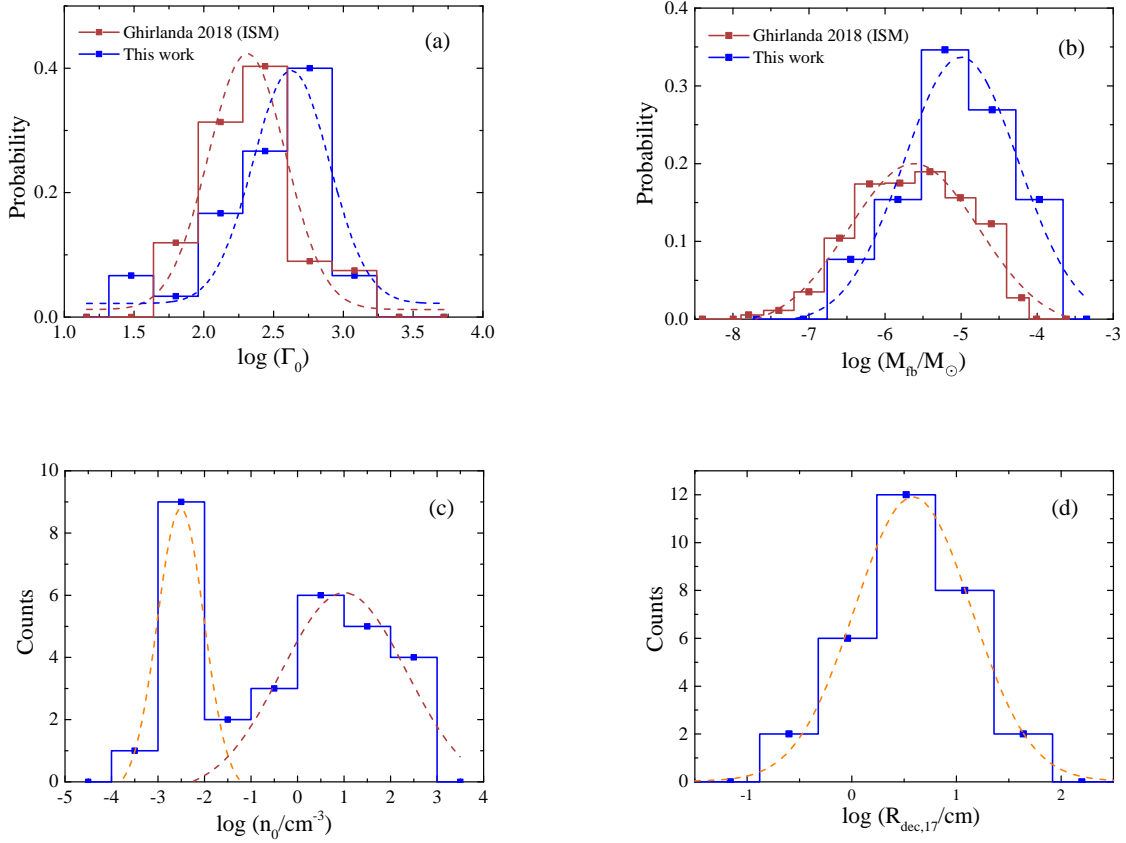


Figure 4. Distributions of $\log \Gamma_0$, $\log(M_{fb}/M_\odot)$, $\log n_0$ and $\log R_{dec,17}$ for the bursts in our sample. The $\log \Gamma_0$ and $\log(M_{fb}/M_\odot)$ distributions taken from Ghirlanda et al. (2018) are also shown with red curves in panels (a) and (b) for comparison. The dashed lines in each panel represent the best fitting of the log-normal/bimodal Gaussian function model.

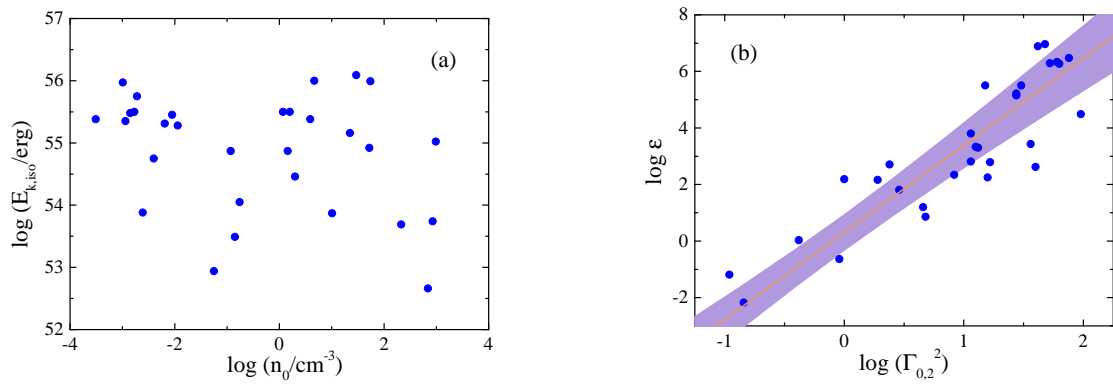


Figure 5. Panel (a)–GRB distribution in the $\log n_0 - \log E_{k,\text{iso}}$ panel for the bursts in our sample. Panel (b)– ε as a function of $\log \Gamma_{0,2}^2$. Their relation derived from the best fit with the OLS bisector algorithm is marked with an orange solid line and its confidence level of 2σ is marked with a purple band.

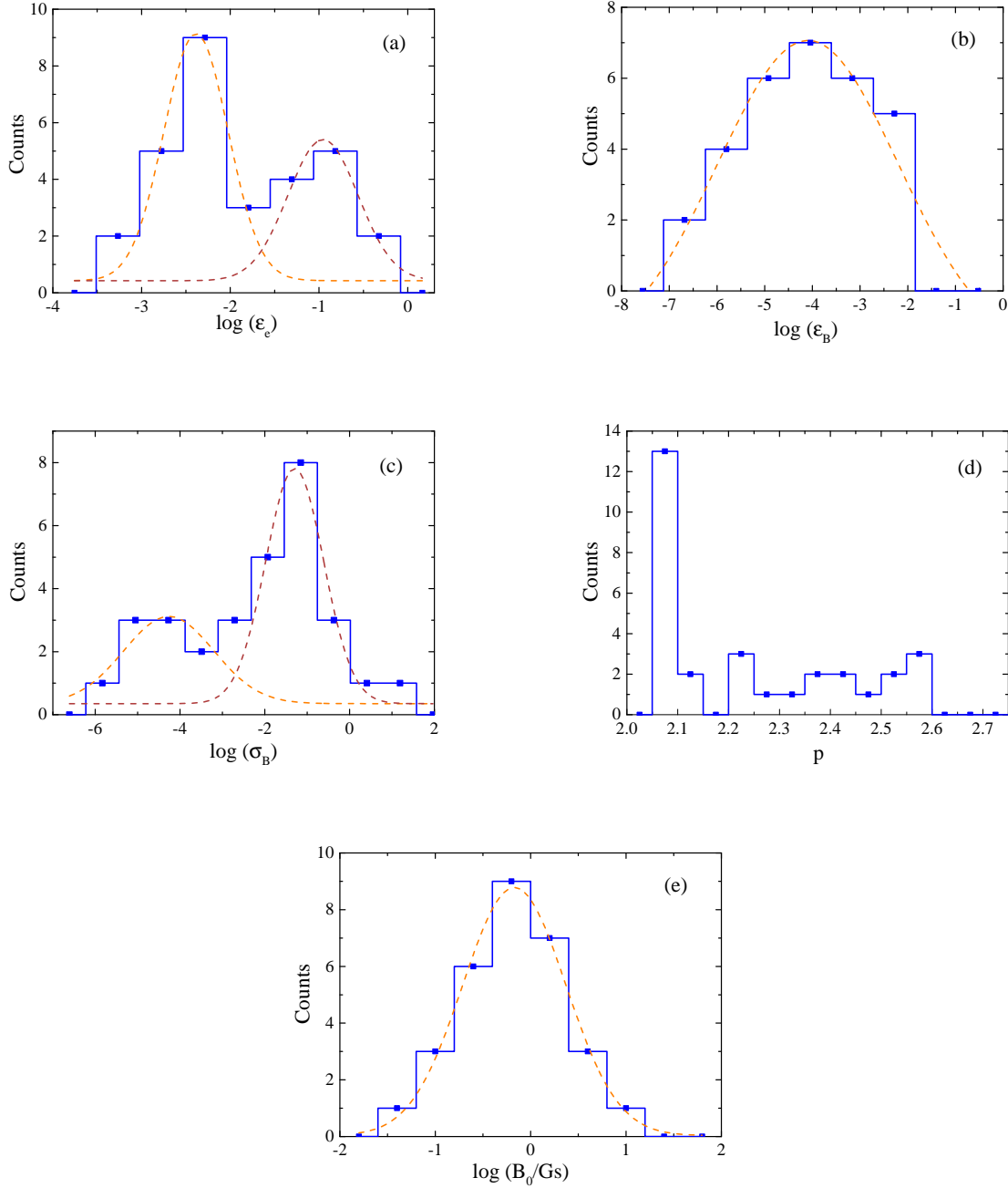


Figure 6. Panel (a)-(e)– Distributions of $\log(\epsilon_e)$, $\log(\epsilon_B)$, $\log(\sigma)$, p and $\log(B_0)$ for the bursts in our sample, respectively. The dashed lines represent the best fitting with a Gaussian function or a two-Gaussian function model.

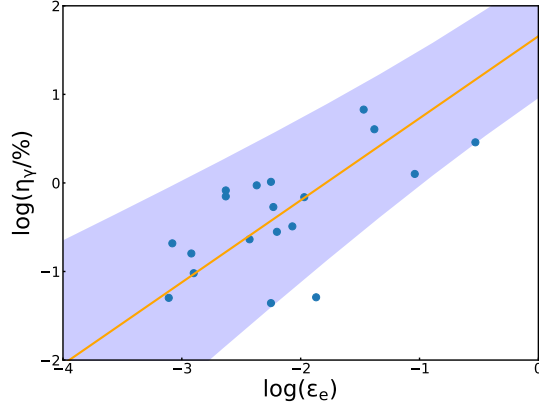


Figure 7. Pair correlations between $\log(\epsilon_e)$ and $\log(\eta_\gamma)$ for the bursts in our sample. The solid line represents the best-fitting result with the OLS bisector algorithm model, and the purple area is the confidence level of 2σ .

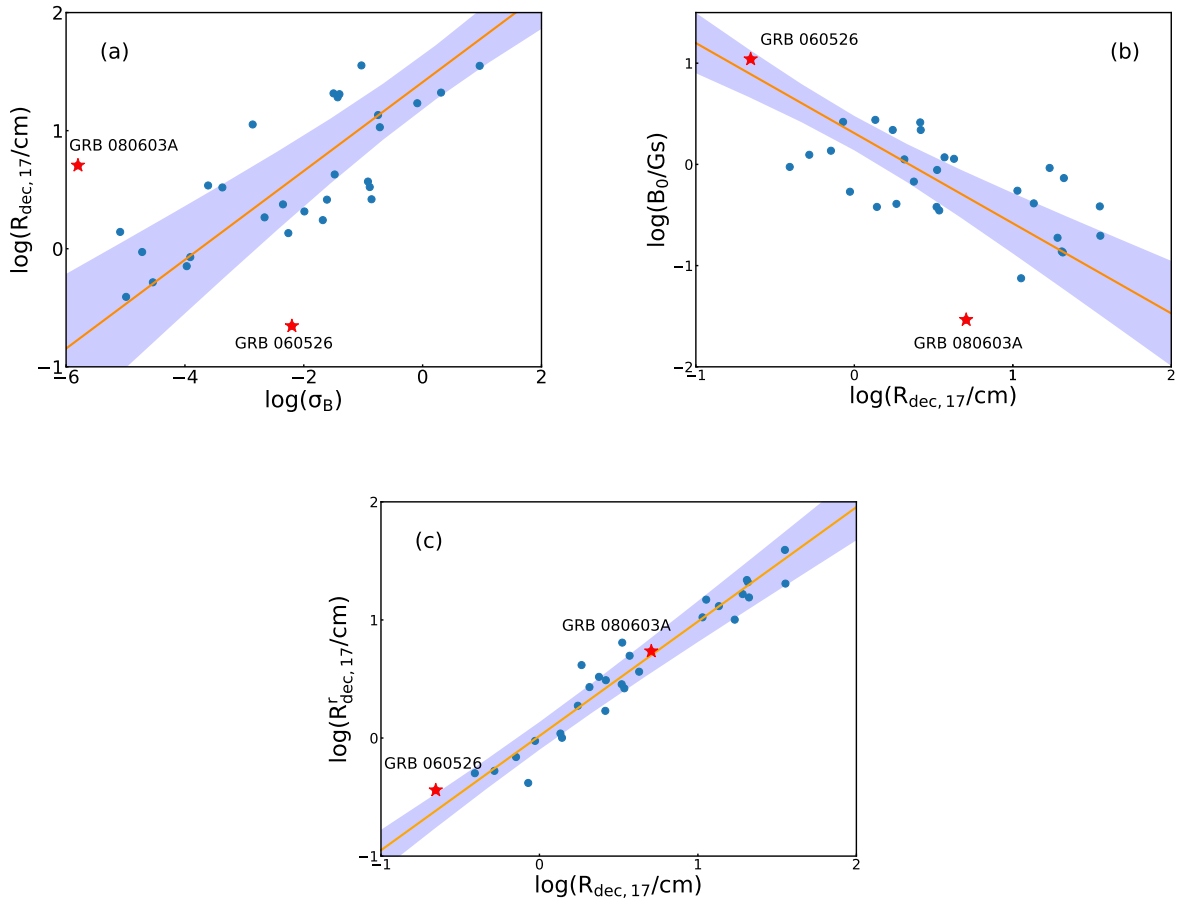


Figure 8. Pair correlations among $R_{\text{dec},17}$, σ_B , B_0 , and the correlation between $R'_{\text{dec},17}(B_0, \sigma_B)$ and $R_{\text{dec},17}$, where $R'_{\text{dec},17}(B_0, \sigma_B)$ is derived from our multiple variable stepwise regression analysis. The red star represents GRBs 060526 and 080603A. The light purple area represents the 2σ confidence level. The orange lines are the best-fitting results by utilizing the OLS bisector.

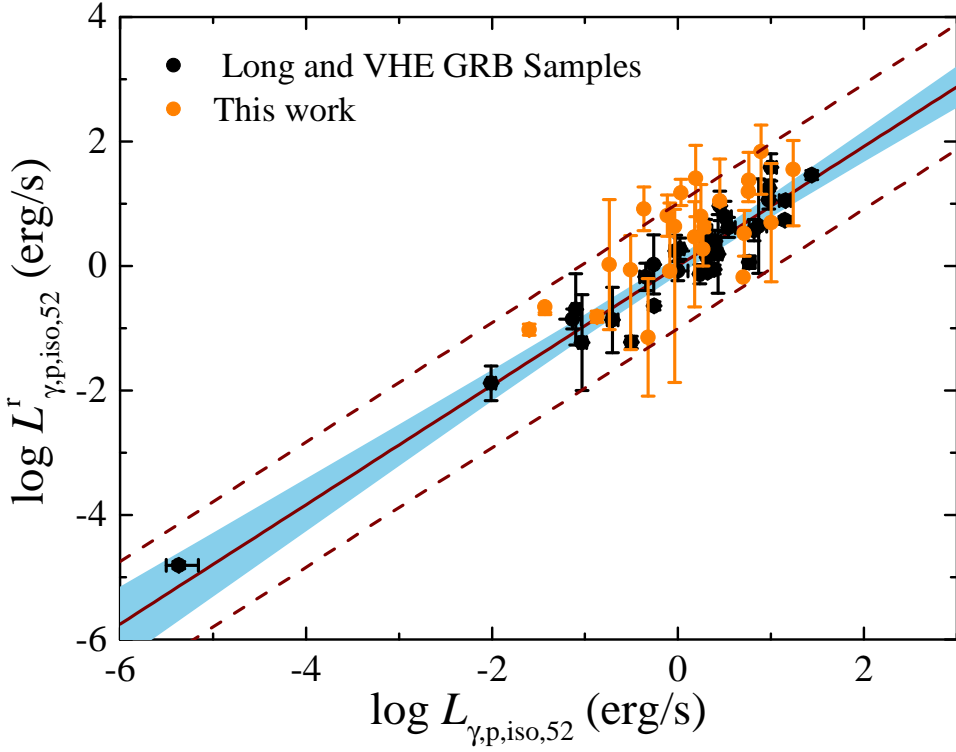


Figure 9. Distribution of the GRBs in our sample (orange dots) in the $\log L_{\gamma,p,\text{iso}}^r - \log L_{\gamma,p,\text{iso}}$ plane, where $\log L_{\gamma,p,\text{iso}}^r$ is calculated with the $L_{\gamma,\text{iso}} - \Gamma_0 - E_{\text{p,z}}$ relation reported by Liang et al. (2015). The typical GRBs, low-luminosity GRBs, high-luminosity GRBs and VHE GRBs from Liang et al. (2015), Huang et al. (2020), and Zhang et al. (2023) are also shown for comparison (black dots). The solid and dashed lines are the best fit and its dispersion in the 3σ confidence level for the relation between $\log L_{\gamma,p,\text{iso}}^r$ and $\log L_{\gamma,p,\text{iso}}$ reported by Liang et al. (2015).